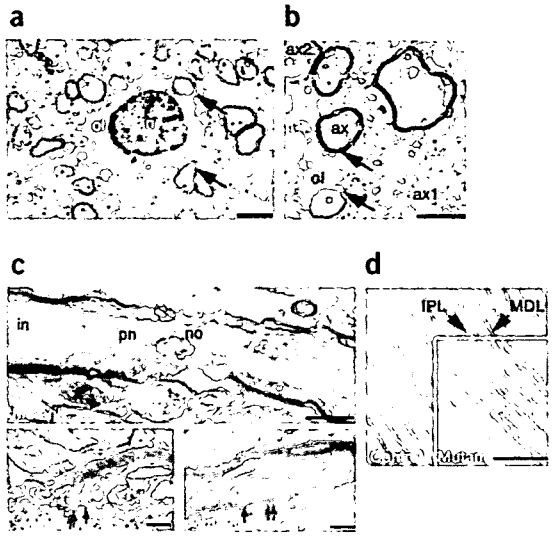

Figure 4 Ultrastructure of oligodendrocytes and myelin. (**a**,**b**) Ultrastructure of the lumbar spinal cord in mutant mice at P9. Mutant oligodendrocytes (ol) show a normal morphology with dark cytoplasm and processes (marked by arrows) that form a thin myelin sheath around associated axons (ax). n, nucleus. Scale bars: **a**, 2 μm; **b**, 1 μm. (**c**) Ultrastructure of the optic nerve from mutant and control mice at P20. Paranodal structures (pn) are well developed in mutant mice (top). Also at higher magnification, paranodes in control (lower left) and mutant (lower right) mice are indistinguishable including the presence of transverse bands, marked by arrows. in, internode; no, node. Scale bars: 1 μm (top) and 0.2 μm (bottom). (**d**) Ultrastructure of the lumbar spinal cord from mutant and control mice at P20. Compact myelin shows the same periodicity with normal major dense line (MDL) and intraperiod lines (IPL) in mutant (inset at lower right) and control mice. Photomicrographs are aligned to show similarity in periodicity. Scale bar, 50 nm.

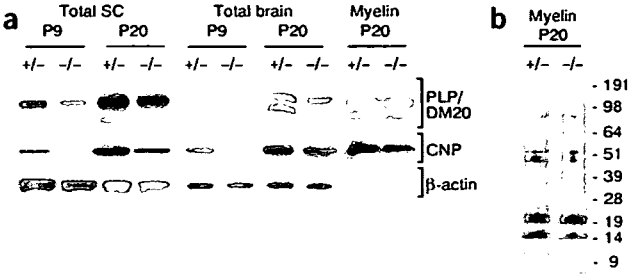

Figure 5 Biochemistry of mutant myelin. (**a**) Western blot comparing the abundance of PLP and CNP in total extracts of spinal cord (Total SC) and brain (Total brain), as well as in purified myelin at the indicated ages. β-actin was used as a loading control. −/−, mutants; +/−, controls. (**b**) Coomassie blue–stained SDS gel (5–12%) of purified myelin membranes of control (+/−) and mutant (−/−) mice. The position of molecular weight marker proteins (in kDa) is indicated.

Ultrastructure of oligodendrocytes and CNS myelin

All oligodendrocytes appeared morphologically healthy, with dark electron-dense cytoplasm and intact organelle structures. Cell nuclei with clumped chromatin[1] (**Fig. 4a**) did not show signs of degeneration. Likewise, we observed oligodendrocyte processes that connected to myelin sheaths surrounding neighboring axons (arrow in **Fig. 4b**). Thus, when in proximity to wild-type neighboring cells, mutant oligodendrocytes survive, mature and are in a position to ensheath axons for myelin assembly.

A critical structure of myelinated axons is the node of Ranvier[19]. Abnormal nodal regions have been described in mice lacking UDP-galactose:ceramide galactosyltransferase (encoded by *Ugt8*; refs. 20,21). In SQS mutants, however, paranodal loops were indistinguishable from those in wild-type mice, and the nodes were of normal size (**Fig. 4c**). The paranodal regions were narrower, reflecting a reduced number of myelin membrane wraps. We rarely observed abnormal nodal structures, such as outwardly directed paranodal loops, a frequent finding in *Ugt8* null mice[20,21] Also, axonal swellings and axonal degeneration, which are seen in young adult PLP- and CNP-deficient myelin mutants[15,22], were not observed in SQS mutants, even at 6 months of age (data not shown).

Theoretically, reducing cholesterol in oligodendroglial membranes could influence the ultrastructure of myelin and its membrane thickness, periodicity and physical compaction. However, mutant myelin membranes had normal periodicity and a regular compaction, as seen by high-power magnification (**Fig. 4d**). Taken together, these results indicate that SQS mutant mice have a previously unknown hypomyelinated phenotype but no obvious ultrastructural defects in the myelin architecture.

Myelin protein composition

We found reduced steady-state levels of myelin proteins in brain and spinal cord extracts by western blotting, as shown for PLP and its splice isoform DM20 (PLP/DM20) and CNP (**Fig. 5a**). When equal amounts of purified myelin proteins were stained with Coomassie blue, the overall pattern appeared the same (**Fig. 5b**), and we confirmed this by western blotting to detect individual proteins (**Fig. 5a**). Thus, myelin membranes were less abundant in mutant brains, but they had a normal protein composition.

Cholesterol in myelin

We expected that genetic disruption of cholesterol biosynthesis would alter the lipid composition of oligodendrocytes and, consequently, of myelin. However, a qualitative comparison of mutant and control myelin lipids by thin-layer chromatography (TLC) showed the same pattern for both mutants and controls (**Fig. 6a**). Indeed, cholesterol was present in CNS myelin from mutant mice, indicating that oligodendrocytes had taken up cholesterol for myelin synthesis.

We quantified lipids in purified myelin by nano-ESI-MS/MS mass spectrometry[23] at P20 (**Supplementary Fig. 2** and **Supplementary Table 1** online). When lipid input was normalized to protein content, mass spectrometry showed a 30% reduction in cholesterol in the myelin of mutants (**Fig. 6b**, upper left). Notably, we did not observe a reduction when the cholesterol content was normalized to other membrane lipids, such as phosphatidylcholine (PC) (**Fig. 6b**, upper right). These data point to an unexpected preservation of the cholesterol-to-lipid stoichiometry and imply a reduced overall ratio of lipid to protein in the myelin of SQS mutant mice as compared to controls. Additionally, a direct comparison of the cholesterol levels in total brain with those in purified myelin showed a major 'enrichment' of cholesterol in myelin, both in mutant mice and in controls (**Fig. 6b**, bottom). This strongly suggests that cholesterol incorporation and enrichment is a requirement for myelin membrane growth, independent of the cellular cholesterol source. Taken together, these results show that in mutant myelin, the ratio of cholesterol to protein is reduced. This reduction is not specific for cholesterol, as it affects all major lipids present almost equally, resulting in a preservation of the normal lipid composition of myelin.

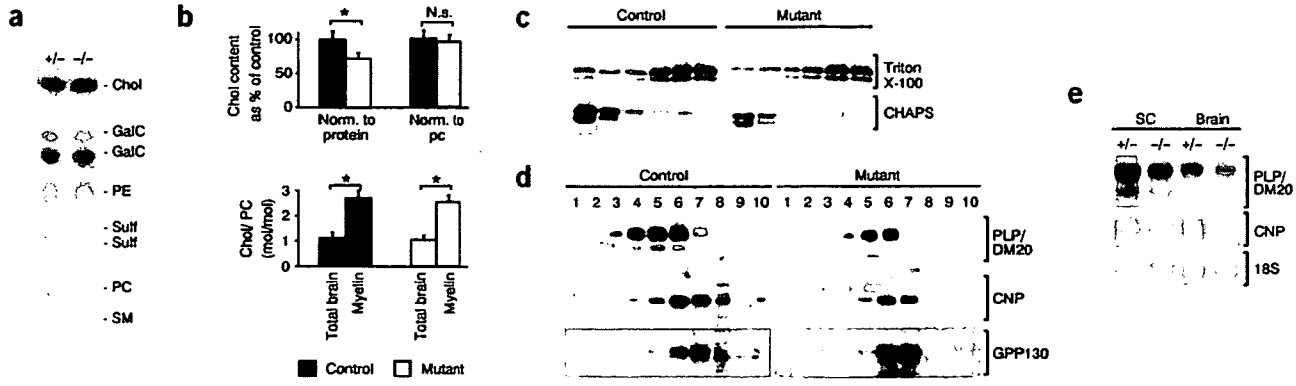

Figure 6 Lipid analysis and detergent-resistant membranes. (**a**) TLC of myelin lipids extracted from purified myelin membranes at P20 (Chol, cholesterol; GalC, galactocerebroside; PE, phosphatidylethanolamin; Sulf, sulfatide; PC, phosphatidylcholine; SM, sphingomyelin). (**b**) Quantitative mass spectrometry of cholesterol and phosphatidylcholine in purified myelin and total brain extracts of P20 animals. Cholesterol content in myelin was normalized to protein input (upper left, mutants: 72.5 ± 7.8%, controls: 100 ± 11.8%) or to phosphatidylcholine (upper right, mutants: 94.9 ± 10.0%). Ratios of cholesterol/ phosphatidylcholine (lower panel) were in determined in myelin (mutants: 2.6 ± 0.26, controls: 2.74 ± 0.31) and total brain extracts (mutants: 1.17 ± 0.15, controls: 1.21 ± 0.12). Values are expressed as mean ± s.e.m. (*$P < 0.005$; N.s., not significant; $n = 5$–6). (**c**) The presence of PLP/DM20 in DRM from myelin (P20). Numbers indicate density gradient fractions, with fractions 1–2 representing floating proteins, and fractions 5–6 representing soluble proteins. (**d**) Density fractions (1–10) of myelin-free microsomes, prepared from total brain at P20, were assessed for the presence of PLP/DM20 and CNP. The Golgi marker GPP130 served as control. (**e**) Northern blot analysis of PLP/DM20 and CNP expression in spinal cord and brain at P20 (18S ribosomal RNA as loading control).

Myelin proteins in DRM complexes

Cholesterol is an essential component of DRM complexes, hypothesized to form membrane lipid rafts[6] and implicated in myelin biogenesis[9]. Lipid alterations could therefore perturb myelination by limiting protein-lipid interactions. We treated myelin membranes with detergents to assess the presence of DRM and analyzed density gradient fractions by western blot (**Fig. 6c**). As previously reported[9], after Triton X-100 treatment, PLP/DM20 was present predominantly in the soluble fractions, whereas after CHAPS treatment, PLP/DM20 containing DRM floated on top of the gradient. This indicates that in mutants and controls, the interaction of PLP/DM20 and lipids within myelin is very similar.

Excess PLP/DM20 not associating with raft lipids could accumulate in a low-cholesterol subcellular compartment. Such retained protein should be found in higher-density fractions than normally sorted protein. To visualize this 'intracellular pool' of myelin proteins, we prepared myelin-free microsomes from total brain lysates and determined their distribution in a density gradient by western blotting (**Fig. 6d**). We detected PLP/DM20 and CNP in equivalent density fractions in mutant and control animals. Thus, PLP/DM20 and CNP are not missorted within mutant oligodendrocytes. However, the steady-state level of the 'intracellular' PLP/CNP pool was lower in mutant brains than in controls (**Fig. 6d**). This suggests a reduced rate of synthesis of myelin proteins. To determine whether the reduction of cellular myelin proteins could be explained by reduced gene expression, we compared PLP/DM20, CNP and myelin basic protein (MBP) mRNA by northern blot. Transcripts in brain and spinal cord were markedly reduced (**Fig. 6e, Supplementary Fig. 3** online and data not shown). Thus, myelin gene expression does not reach its normal peak when cholesterol is limited. This may protect oligodendrocytes from the harmful effects of myelin protein overexpression[22,24,25]. Taken together, these results indicate that cholesterol and myelin lipids associate with PLP in oligodendrocytes, forming DRM complexes ('myelin rafts') with normal biochemical features in mutant mice. However, the reduced availability of cholesterol inhibits high protein expression, possibly at the transcriptional level.

Overcoming dysmyelination by cholesterol uptake

We noticed that the trembling phenotype of mutant mice improved with age. Additionally, silver impregnation of myelin at P100 no longer showed substantial differences between mutant mice and controls (**Fig. 7a**). That was confirmed by western blot analysis: the reduced amounts of myelin proteins seen at P20 were not seen to the same extent at P100 (data not shown). At 3 months, virtually all medium- and large-caliber axons in the spinal cord were myelinated, as shown by electron microscopy, although myelin thickness in the white matter was still below that of controls (**Fig. 7b**).

Astrocytes are a reported source of cholesterol for cultured neurons[26], but whether astrocytes deliver cholesterol *in vivo* to oligodendrocytes is not known. When tissue sections were immunostained for the astroglial marker glial fibrillary acidic protein (GFAP), we observed astrogliosis in mutant spinal cord gray matter at P20 that persisted for at least 6 months (**Fig. 7c**). However, no such astroglial hyperplasia was observed in spinal cord or subcortical white matter. Additionally, immunostaining for macrophage differentiation antigen 3 (MAC-3), a marker of microglia, showed little gliosis (data not shown). Co-staining showed that some GFAP-positive astrocytes in subcortical white matter express HMG CoA reductase, the rate-limiting enzyme of cholesterol synthesis. These astrocytes are in a position to provide cholesterol to mutant oligodendrocytes (**Supplementary Fig. 4** online). The most abundant lipoprotein particles in the CNS contain apolipoprotein E (ApoE), of which astrocytes and microglia are well-known sources[26,27]. In mutants, we found slightly increased steady-state levels of ApoE upon western blotting (**Fig. 7d**), suggestive of enhanced disposal of cholesterol-containing lipoprotein particles. Additionally, low-density lipoprotein receptor related protein (LRP) is one of the major receptors of cholesterol-loaded lipoproteins in the CNS[27]. By western blotting, we found more LRP in the spinal cord of mutant mice than in controls (**Fig. 7d**); it was also expressed in oligodendrocytes, as determined by *in situ* hybridization (data not shown). Thus, LRP is a candidate for cholesterol uptake by mutant oligodendrocytes. These data imply an enhanced horizontal transfer of cholesterol through lipoprotein particles in mutant animals.

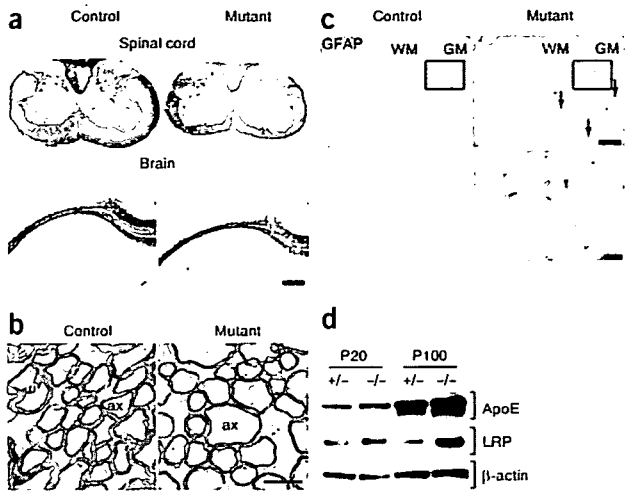

Figure 7 Natural compensation for cholesterol deficiency. (**a**) Histological analysis of adult mice (P100) using Gallyas silver impregnation of myelin (scale bar, 400 μm). (**b**) Ultrastructural analysis of white matter of lumbar spinal cord at P100 confirmed that, as in control animals, all axons (ax) in mutant mice were myelinated (m, myelin). Nevertheless, myelination did not reach control levels (scale bar, 1 μm). (**c**) Astrogliosis in the spinal cord of mutant mice (P20) is shown by an increase in GFAP-positive cells (arrows). Lower panels show an enlarged view of the boxed areas of gray matter (WM, white matter; GM, gray matter; scale bars: upper panel, 50 μm, lower panel, 10 μm). (**d**) Apolipoprotein E (ApoE) and low-density lipoprotein receptor related protein (LRP) were slightly more abundant in mutant (−/−) animals than in control (+/−) animals, as assessed by western blotting in total lysates of spinal cord. β-actin was used as a loading control.

DISCUSSION

We have aimed to elucidate the function of cholesterol in mammalian development *in vivo*. As cholesterol is essential for embryonic development[13], we have developed conditional mouse mutants by Cre-mediated targeting of the *Fdft1* gene. By specifically inactivating *Fdft1* in oligodendrocytes, we were able to observe the first cell type–specific inactivation of cholesterol biosynthesis *in vivo* and describe a previously unknown, informative phenotype. An obvious feature of the conditional mutants is a severely reduced rate of myelination in white matter. This proves unequivocally that the bulk of cholesterol incorporated into myelin is made by oligodendrocytes. The data also demonstrate an efficient horizontal transfer of cholesterol between different brain cell types, which is relevant to neurodegenerative diseases. That mutant oligodendrocytes depend on the local supply of cholesterol is supported by the unexpected finding that purified myelin from mutant mice has an almost normal composition of proteins and lipids, including the characteristic high cholesterol level. Myelin cannot be synthesized without cholesterol, or even with the normal cholesterol content of plasma membranes; only a moderate reduction of the cholesterol-to-protein ratio is tolerated. Thus, the availability of cholesterol is an essential, rate-limiting factor for myelin growth.

Oligodendrocyte survival

The emergence of oligodendrocyte precursors requires the expression of *Olig1* and *Olig2*, which is dependent on sonic hedgehog (Shh)[28]. Theoretically, dysmyelination could result from a defect in cholesterol-dependent Shh signaling and from a diminished number of newly generated oligodendrocytes. This is unlikely, however, because CNP promoter activity begins only in committed oligodendrocyte precursors, which are Shh independent[29,30]. In fact, pre-existing levels of SQS in newly generated oligodendrocytes may allow for some cholesterol biosynthesis until the onset of myelination.

When cholesterol synthesis is blocked by enzymatic inhibitors, the accumulation of metabolites can be cytotoxic[31,32]. However, we did not find an accumulation of such metabolites by mass spectroscopy (data not shown). Although we cannot formally exclude their abnormal formation, it is more likely that these lipid metabolites do not occur or are efficiently cleared. We occasionally noticed amorphous inclusions in the cytoplasm of some mutant oligodendrocytes by electron microscopy (data not shown). The nature of the aggregates is presently unknown, but they are unlikely to cause the observed phenotype of mutant mice.

Horizontal cholesterol transfer

The net transfer of cholesterol from wild-type cells to SQS-deficient oligodendrocytes is notable, given the extent of myelination in some brain areas. It is likely that some oligodendrocytes (in cortical gray matter, for example) are 'privileged' because of the numerous neighboring wild-type cells, such as astrocytes. We have found increased steady-state levels of ApoE and LRP, suggesting an enhanced lipoprotein particle–mediated cholesterol transfer in mutant mice. Whether levels of these particles are rate limiting for myelination in mutants remains to be determined. Given the overall low level of ApoE and LRP, horizontal cholesterol transfer may also involve other still undefined mechanisms. High dietary cholesterol did not influence the developmental delay of mutant mice (**Supplementary Fig. 5** online), suggesting that bulk transfer of cholesterol from the periphery is not responsible for myelination in mutant mice.

Cholesterol-dependent dysmyelination

The 'checkpoints' at which normal cholesterol levels are required may involve more than one molecular mechanism. Myelin is assembled by vesicular trafficking of membranes that contain myelin-specific proteins, glycolipids and cholesterol[7,8]. A critical stoichiometry of lipid and protein could be controlled within a late Golgi compartment or within a sorting endosome. The association of cholesterol with myelin proteins could stabilize a conformation that is required for further transport to the myelin compartment. We were surprised to find that PLP/DM20 was contained in DRM complexes from SQS mutant mice in equal amounts as in controls (that is, in total brain extracts, purified myelin and brain microsomes). Thus, raft formation in mutant oligodendrocytes is not impaired and PLP/DM20 not missorted.

In mutant oligodendrocytes, the pool of microsomal (that is, cellular) myelin proteins and their corresponding mRNAs did not reach normal peak levels. We hypothesize that oligodendrocytes sense the mismatch in the protein/cholesterol ratio and react by attenuating myelin gene expression accordingly. Normally, the level of cholesterol in membranes is tightly regulated by sterol regulatory element–binding transcription factor 2 (SREBP-2), a cholesterol-regulated transcription factor[33]. In the course of Schwann cell development, SREBP-2 expression is correlated with the concerted expression of myelin lipids[34]. Whether coordinating the ratio of myelin proteins to lipids involves SREBP function needs to be explored. Notably, the transcription of HMG-CoA reductase, a direct SREBP target, is not upregulated in oligodendrocytes (**Supplementary Fig. 4**).

Steroid hormones such as progesterone are made by oligodendrocytes, and progesterone stimulates myelin gene expression[35]. The lack of cholesterol biosynthesis could diminish steroid hormone levels, leading secondarily to hypomyelination, but that seems unlikely.

We found the same level of progesterone in brain lysates from mutants (6.0 ± 0.65 ng per g protein) and controls (6.4 ± 0.6 ng per g protein), suggesting that brain progesterone levels are not limiting.

Comparison with other myelin mutant mice

Hypomyelination is a well-known phenotype of mice with gain-of-function mutations in myelin protein genes[36]. In the complete absence of most myelin proteins, including PLP/DM20, MOG, P0, OSP (claudin-11), MAL and PMP22 (ref. 36), significant myelin assembly is possible. To our knowledge, MBP is the only myelin component beside cholesterol that is required and rate-limiting for myelin membrane growth[25,37].

Previous genetic approaches to study the function of lipids in myelin have involved two myelin-specific glycolipids: galactocerebroside (GalC) and its sulfated derivative[20,21]. Myelination is not prevented in these mutant mice, which have a complex phenotype with signs of dysmyelination and demyelination. Indeed, myelin gene expression remains high in GalC-deficient oligodendrocytes, despite an altered myelin lipid profile[20,21]. An important phenotype of GalC-deficient mice is the instability of paranodal junctions, which reduces the insulating capacity of myelin[20,21], a feature not found in SQS mutant mice.

Implication for human cholesterol deficiency diseases

Several genetic disorders of the cholesterol biosynthetic pathway have been reported in humans. They are associated with myelination defects but also include complex craniofacial malformations[38]. Mouse mutants lacking 7-dehydrocholesterol reductase (*Dhcr7*$^{-/-}$) are a model for human Smith-Lemli-Opitz-syndrome[31], and mutants lacking 24-dehydrocholesterol reductase (*Dhcr24*$^{-/-}$) are a model of desmosterolosis[39]. Both genetic disorders affect the last steps of cholesterol biosynthesis, and the phenotypes are also determined by the presence of precursor sterols.

Sterol precursors cannot fully substitute for cholesterol itself and may exert harmful effects[31]. Thus, to understand normal cholesterol biology, it is an advantage that SQS-deficient mutants show no compensation by cholesterol-like precursors. We anticipate that floxed SQS mice, when combined with different patterns of Cre expression in the brain, will allow systematic exploration of the biological function of cholesterol *in vivo*, aspects of horizontal cholesterol transfer and the effect of pharmacological interventions.

METHODS

Molecular cloning. A targeting vector for the mouse *Fdft1* gene was constructed with Sv129 genomic DNA extending from intron 4 to intron 7 and was cloned into a modified pGEM3Zf(+) vector (Promega). One *lox*P site was inserted 5′ to exon 5 using a *Bam*HI site. A neomycin selection cassette and the second *lox*P site were introduced 3′ to exon 5 using an *Eco*RV site.

Mouse genetics. All animal experiments were approved by the state of Niedersachsen, Germany. Positively selected embryonic stem cell clones (E14.1Sv129/OLA, kindly provided by N. Brose, Max Planck Institute of Experimental Medicine, Goettingen, Germany) were identified by PCR. All primer sequences are available upon request. To verify single transgene integration, we performed genomic Southern blotting using a radiolabeled probe of the *neo* resistance gene. C57Bl/6J blastocyst injection was done as previously described[40]. Progeny of a chimera with germline transmission gave rise to the SQS-flox mouse line. For genotyping, genomic DNA was isolated from tail biopsies using the DNeasy 96 tissue kit (Qiagen) and analyzed by PCR. To minimize possible influences of the genetic background, mutants and control littermates were analyzed. Survival curves were calculated according to Kaplan-Meier.

Motor performance assay. Motor coordination and balance were measured by performance on the rotarod[41]. Briefly, after placing mice on a rod, rotation was initiated with increasing speeds from 2–20 rpm in 60 s intervals and latency to fall was recorded (trial completion, 300 s). Values are expressed as mean ± s.e.m.

RNA analysis. For northern blotting, brain RNA purification and hybridization was done as described[15] using radiolabeled probes corresponding to mouse PLP or CNP coding sequences. For *in situ* hybridization, digoxigenin UTP–labeled cRNA probes were generated using a labeling kit (Promega). *In situ* hybridization was performed as described[42].

Antibodies. Antibodies detecting the following proteins were used: SQS (Becton & Dickinson) 1:1,000; CNP (Sigma) 1:300; Cre and GPP130 (Babco) both 1:500; MAG (Chemicon) 1:500 or 1:20 (ref. 43); PLP-A431 (ref. 44) 1:500; Actin (Sigma) 1:1,000; LRP (Transduction Laboratories) 1:200; and GFAP (Chemicon) 1:500.

Protein analysis. For total lysates, whole brains (1:10 wt/vol) were homogenized on ice in lysis buffer (1% Triton X-100, 20 mM Tris-HCl pH 8.0, 137 mM NaCl, 2 mM EDTA, with protease inhibitors (Complete, Roche)). Myelin membranes were purified as described[45]. Detection of immunolabeled protein was performed using chemiluminescence (NEN Life Science Products). Representative results from at least three independent experiments are shown.

Preparation of DRM fractions. DRM assays of purified myelin membranes were performed as described[9,46]. To prepare intracellular membranes, we isolated brain microsomes by differential centrifugation after the removal of myelin membranes[47] and processed them as described[48].

Histology and electron microscopy. On paraffin-embedded tissue sections (4 μm), we visualized myelinated fibers by Gallyas silver impregnation[18]. For immunohistochemistry, we used the Dako-LSAB$_2$ system (Dako), or standard procedures[43] for the analysis of MAG. Sections were analyzed by light microscopy (Zeiss Axiophot). For electron microscopy, we embedded perfused tissue in epoxy resin (Serva) as described[15], before examination (EM912AB, Leo).

Lipid analysis. Total lipid extracts of CNS myelin were made by standard procedures[49], and processed for TLC as described[9]. Progesterone in total brain lysates was measured using the Elecsys progesterone chemiluminescence assay (Roche).

Mass spectrometry. Electrospray ionization (ESI) coupled with collision-induced dissociation (CID) and mass spectrometry (either MS/MS or time-of-flight) was performed as described[23]. Cholesterol was normalized to either protein or phosphatidylcholine contents. Values were expressed as mean percentages of control contents ± s.e.m. Significance was determined using Student's *t*-test of two-tailed uncoupled samples.

Note: Supplementary information is available on the Nature Neuroscience website.

ACKNOWLEDGMENTS

We dedicate this work to P. Morell for his pioneering work on brain cholesterol synthesis. We thank L. Bitterberg, A. Fahrenholz, S. Keese, I. Leibrecht, E. Nicksch and M. Schindler for excellent technical help; M. Schwab for providing us with antibodies; and M. Simons for helpful comments on the manuscript. This work was supported by the Deutsche Forschungsgemeinschaft (SFB523 to K.A.N.; Wi654/7 to B.B. and F.W.), the Hertie Institute of Multiple Sclerosis Research and grants from the European Union (K.A.N.).

COMPETING INTERESTS STATEMENT

The authors declare that they have no competing financial interests.

Received 26 January; accepted 25 February 2005
Published online at http://www.nature.com/natureneuroscience/

1. Peters, A., Palay, S.L. & Webster, H.D. *The Fine Structure of the Nervous System— the Neurons and Supporting Cells* 3rd edn. (Oxford Univ. Press, New York, 1991).
2. Morell, P. & Jurevics, H. Origin of cholesterol in myelin. *Neurochem. Res.* **21**, 463–470 (1996).
3. Ohvo-Rekila, H., Ramstedt, B., Leppimaki, P. & Slotte, J.P. Cholesterol interactions with phospholipids in membranes. *Prog. Lipid Res.* **41**, 66–97 (2002).
4. Haines, T.H. Do sterols reduce proton and sodium leaks through lipid bilayers? *Prog. Lipid Res.* **40**, 299–324 (2001).

5. Brown, D.A. & London, E. Structure and function of sphingolipid- and cholesterol-rich membrane rafts. *J. Biol. Chem.* **275**, 17221–17224 (2000).
6. Simons, K. & Toomre, D. Lipid rafts and signal transduction. *Nat. Rev. Mol. Cell Biol.* **1**, 31–39 (2000).
7. Kramer, E.M., Schardt, A. & Nave, K.A. Membrane traffic in myelinating oligodendrocytes. *Microsc. Res. Tech.* **52**, 656–671 (2001).
8. Larocca, J.N. & Rodriguez-Gabin, A.G. Myelin biogenesis: vesicle transport in oligodendrocytes. *Neurochem. Res.* **27**, 1313–1329 (2002).
9. Simons, M., Kramer, E.M., Thiele, C., Stoffel, W. & Trotter, J. Assembly of myelin by association of proteolipid protein with cholesterol- and galactosylceramide-rich membrane domains. *J. Cell Biol.* **151**, 143–154 (2000).
10. Michikawa, M. & Yanagisawa, K. Inhibition of cholesterol production but not of nonsterol isoprenoid products induces neuronal cell death. *J. Neurochem.* **72**, 2278–2285 (1999).
11. Bradfute, D.L., Silva, C.J. & Simoni, R.D. Squalene synthase-deficient mutant of Chinese hamster ovary cells. *J. Biol. Chem.* **267**, 18308–18314 (1992).
12. Ohashi, K. *et al.* Early embryonic lethality caused by targeted disruption of the HMG-CoA reductase gene. *J. Biol. Chem.* **278**, 42936–42941 (2003).
13. Tozawa, R. *et al.* Embryonic lethality and defective neural tube closure in mice lacking squalene synthase. *J. Biol. Chem.* **274**, 30843–30848 (1999).
14. Gu, P., Ishii, Y., Spencer, T.A. & Shechter, I. Function-structure studies and identification of three enzyme domains involved in the catalytic activity in rat hepatic squalene synthase. *J. Biol. Chem.* **273**, 12515–12525 (1998).
15. Lappe-Siefke, C. *et al.* Disruption of Cnp1 uncouples oligodendroglial functions in axonal support and myelination. *Nat. Genet.* **33**, 366–374 (2003).
16. Genoud, S. *et al.* Notch1 control of oligodendrocyte differentiation in the spinal cord. *J. Cell Biol.* **158**, 709–718 (2002).
17. Belachew, S., Yuan, X. & Gallo, V. Unraveling oligodendrocyte origin and function by cell-specific transgenesis. *Dev. Neurosci.* **23**, 287–298 (2001).
18. Gallyas, F. Silver staining of myelin by means of physical development. *Neurol. Res.* **1**, 203–209 (1979).
19. Salzer, J.L. Polarized domains of myelinated axons. *Neuron* **40**, 297–318 (2003).
20. Marcus, J. & Popko, B. Galactolipids are molecular determinants of myelin development and axo-glial organization. *Biochim. Biophys. Acta* **1573**, 406–413 (2002).
21. Stoffel, W. & Bosio, A. Myelin glycolipids and their functions. *Curr. Opin. Neurobiol.* **7**, 654–661 (1997).
22. Nave, K.A. & Griffiths, I.R. Models of Pelizaeus-Merzbacher disease. in *Myelin Biology and Disorders* Vol. 2 (ed. Lazzarini, R.A.) 1125–1142 (Academic, London, 2003).
23. Sandhoff, R., Brügger, B., Jeckel, D., Lehmann, W.D. & Wieland, F.T. Determination of cholesterol at the low picomole level by nano-electrospray ionization tandem mass spectrometry. *J. Lipid Res.* **40**, 126–132 (1999).
24. Simons, M. *et al.* Overexpression of the myelin proteolipid protein leads to accumulation of cholesterol and proteolipid protein in endosomes/lysosomes: implications for Pelizaeus-Merzbacher disease. *J. Cell Biol.* **157**, 327–336 (2002).
25. Readhead, C. *et al.* Expression of a myelin basic protein gene in transgenic shiverer mice: correction of the dysmyelinating phenotype. *Cell* **48**, 703–712 (1987).
26. Pfrieger, F.W. Outsourcing in the brain: do neurons depend on cholesterol delivery by astrocytes? *Bioessays* **25**, 72–78 (2003).
27. Herz, J. & Bock, H.H. Lipoprotein receptors in the nervous system. *Annu. Rev. Biochem.* **71**, 405–434 (2002).
28. Lu, Q.R. *et al.* Sonic hedgehog–regulated oligodendrocyte lineage genes encoding bHLH proteins in the mammalian central nervous system. *Neuron* **25**, 317–329 (2000).
29. Alberta, J.A. *et al.* Sonic hedgehog is required during an early phase of oligodendrocyte development in mammalian brain. *Mol. Cell. Neurosci.* **18**, 434–441 (2001).
30. Cooper, M.K. *et al.* A defective response to Hedgehog signaling in disorders of cholesterol biosynthesis. *Nat. Genet.* **33**, 508–513 (2003).
31. Nwokoro, N.A., Wassif, C.A. & Porter, F.D. Genetic disorders of cholesterol biosynthesis in mice and humans. *Mol. Genet. Metab.* **74**, 105–119 (2001).
32. Kim, S.U. Effects of the cholesterol biosynthesis inhibitor ay9944 on organotypic cultures ofmouse spinal cord. Retarded myelinogenesis and induction of cytoplasmic inclusions. *Lab. Invest.* **32**, 720–728 (1975).
33. Brown, M.S. & Goldstein, J.L. A proteolytic pathway that controls the cholesterol content of membranes, cells, and blood. *Proc. Natl. Acad. Sci. USA* **96**, 11041–11048 (1999).
34. Verheijen, M.H., Chrast, R., Burrola, P. & Lemke, G. Local regulation of fat metabolism in peripheral nerves. *Genes Dev.* **17**, 2450–2464 (2003).
35. Sereda, M.W., Meyer Zu, H.G., Suter, U., Uzma, N. & Nave, K.A. Therapeutic administration of progesterone antagonist in a model of Charcot-Marie-Tooth disease (CMT-1A). *Nat. Med.* **9**, 1533–1537 (2003).
36. Lazzarini, R.A. *Myelin Biology and Disorders* (Academic, London, 2003).
37. Popko, B. *et al.* Myelin deficient mice: expression of myelin basic protein and generation of mice with varying levels of myelin. *Cell* **48**, 713–721 (1987).
38. Bjorkhem, I. & Meaney, S. Brain cholesterol: long secret life behind a barrier. *Arterioscler. Thromb. Vasc. Biol.* **24**, 806–815 (2004).
39. Wechsler, A. *et al.* Generation of viable cholesterol-free mice. *Science* **302**, 2087 (2003).
40. Joyner, A.L. Gene targeting and gene trap screens using embryonic stem cells: new approaches to mammalian development. *Bioessays* **13**, 649–656 (1991).
41. Jones, B.J. & Roberts, D.J. A rotarod suitable for quantitative measurements of motor incoordination in naive mice. *Naunyn Schmiedebergs Arch. Exp. Pathol. Pharmakol.* **259**, 211 (1968).
42. Schaeren-Wiemers, N. & Gerfin-Moser, A. A single protocol to detect transcripts of various types and expression levels in neural tissue and cultured cells: *in situ* hybridization using digoxigenin-labelled cRNA probes. *Histochemistry* **100**, 431–440 (1993).
43. Huber, A.B., Weinmann, O., Brosamle, C., Oertle, T. & Schwab, M.E. Patterns of Nogo mRNA and protein expression in the developing and adult rat and after CNS lesions. *J. Neurosci.* **22**, 3553–3567 (2002).
44. Jung, M., Sommer, I., Schachner, M. & Nave, K.A. Monoclonal antibody O10 defines a conformationally sensitive cell-surface epitope of proteolipid protein (PLP): evidence that PLP misfolding underlies dysmyelination in mutant mice. *J. Neurosci.* **16**, 7920–7929 (1996).
45. Norton, W.T. & Poduslo, S.E. Myelination in rat brain: method of myelin isolation. *J. Neurochem.* **21**, 749–757 (1973).
46. Brown, D.A. & Rose, J.K. Sorting of GPI-anchored proteins to glycolipid-enriched membrane subdomains during transport to the apical cell surface. *Cell* **68**, 533–544 (1992).
47. Jurevics, H. *et al.* Normal metabolism but different physical properties of myelin from mice deficient in proteolipid protein. *J. Neurosci. Res.* **71**, 826–834 (2003).
48. Plonne, D. *et al.* Separation of the intracellular secretory compartment of rat liver and isolated rat hepatocytes in a single step using self-generating gradients of iodixanol. *Anal. Biochem.* **276**, 88–96 (1999).
49. Bligh, E.G. & Dyer, W.J. A rapid method of total lipid extraction and purification. *Can. J. Med. Sci.* **37**, 911–917 (1959).

Disruption of Autosomal Recessive Hypercholesterolemia Gene Shows Different Phenotype In Vitro and In Vivo

Mariko Harada-Shiba, Atsuko Takagi, Kousuke Marutsuka, Sayaka Moriguchi, Hiroaki Yagyu, Shun Ishibashi, Yujiro Asada, Shinji Yokoyama

Abstract—We previously characterized the patients with autosomal recessive hypercholesterolemia (ARH) as having severe hypercholesterolemia and retarded plasma low-density lipoprotein (LDL) clearance despite normal LDL receptor (LDLR) function in their cultured fibroblasts, and we identified a mutation in the *ARH* locus in these patients. ARH protein is an adaptor protein of the LDL and reportedly modulates its internalization. We developed ARH knockout mice ($ARH^{-/-}$) to study the function of this protein. Plasma total cholesterol level was higher in $ARH^{-/-}$ mice than that in wild-type mice ($ARH^{+/+}$), being attributed to a 6-fold increase of LDL, whereas plasma lipoprotein was normal in the heterozygotes ($ARH^{+/-}$). Clearance of ^{125}I-LDL from plasma was retarded in $ARH^{-/-}$ mice, as much as that found in $LDLR^{-/-}$ mice. Fluorescence activity of the intravenously injected 1,1′-dioctadecyl-3,3,3′,3′-tetramethylindocarbocyanine perchlorate (DiI)-LDL was recovered in the cytosol of the hepatocytes of $ARH^{+/+}$ mice, but not in those of $ARH^{-/-}$ or $LDLR^{-/-}$ mice. Also, less radioactivity was recovered in the liver of $ARH^{-/-}$ or $LDLR^{-/-}$ mice when [^{3}H]cholesteryl oleyl ether (CE)-labeled LDL was injected. In contrast, uptakes of [^{3}H]CE-labeled LDL, ^{125}I-LDL, and DiI-LDL were all normal or slightly subnormal when the $ARH^{-/-}$ hepatocytes were cultured. We thus concluded that the function of the hepatic LDLR is impaired in the $ARH^{-/-}$ mice in vivo, despite its normal function in vitro. These findings were consistent with the observations with the ARH homozygous patients and suggested that certain cellular environmental factors modulate the requirement of ARH for the LDLR function. **(*Circ Res.* 2004;95:945-952.)**

Key Words: autosomal recessive hypercholesterolemia ■ knockout mouse ■ low-density lipoprotein receptor ■ primary cultured hepatocytes ■ OmniBank

Hereditary hypercholesterolemia was first characterized by Khachadurian and Kuthman in 1973[1] as severe hypercholesterolemia with cutaneous and tendon xanthomas and premature atherosclerosis. They proposed two categories, autosomal dominant and recessive.[1] Hypercholesterolemia with autosomal dominant inheritance was termed familial hypercholesterolemia. Studies of familial hypercholesterolemia led to the discovery of low-density lipoprotein receptor (LDLR) and identification of its genetic dysfunction as the cause of this disease. The LDLR is now known to play a key role in the internalization of LDL into the cell and in the regulation of plasma LDL concentrations.[2,3] However, hypercholesterolemia with autosomal recessive inheritance had never been fully characterized until we first reported this disease.[4,5] In these articles, we described siblings with severe hypercholesterolemia, exhibiting huge xanthomas and premature atherosclerosis despite normal LDLR activity in their cultured fibroblasts.

In 2001, Garcia et al[6] mapped the *ARH* locus to chromosome 1p35 using six families of autosomal recessive hypercholesterolemia (ARH). They identified six mutations of the gene encoding a putative LDLR adaptor protein in these ARH families. We showed that an insertion mutation in the *ARH* gene of the Japanese siblings described causes an early stop codon.[7]

ARH protein has an N-terminal phosphotyrosine-binding (PTB) domain.[6] The PTB domain is found in several adaptor proteins, such as Disabled-2 and numb, and binds to an NPXY sequence in the cytoplasmic tails of cell surface receptors to modulate their internalization. Recently, the PTB domain of ARH protein was shown by the pull-down technique to bind to the FDNPVY sequence of LDLR.[8] ARH protein was also reported to interact with clathrin and is thought to function as an adaptor protein that couples LDLR to the endocytic machinery.[8]

What is unique about the patients with ARH is the apparent inconsistency of the LDLR functions between in vitro and in

Original received October 24, 2003; resubmission received June 10, 2004; revised resubmission received September 13, 2004; accepted September 24, 2004.

From the Department of Bioscience (M.H.-S.), Department of Pharmacology (A.T.), National Cardiovascular Center Research Institute, Osaka; First Department of Pathology (K.M., S.M., Y.A.), Miyazaki Medical College, Miyazaki; Division of Endocrinology and Metabolism (H.Y., S.I.), Jichi Medical School, Kawachi-gun, Tochigi; Department of Biochemistry, Cell Biology, and Metabolism (S.Y.), Nagoya City University Graduate School of Medical Sciences, Mizuho-cho, Nagoya, Aichi, Japan.

Correspondence to Mariko Harada-Shiba, Department of Bioscience, National Cardiovascular Center Research Institute, Fujishiro-dai, Suita, Osaka 565-8565, Japan. E-mail mshiba@ri.ncvc.go.jp

Circulation Research is available at http://www.circresaha.org DOI: 10.1161/01.RES.0000146946.78540.46

vivo. In ARH patients, clearance of ^{125}I-LDL from plasma is delayed to the same extent as that found among homozygous familial hypercholesterolemia, whereas LDL binding, internalization, and degradation are normal or subnormal in their cultured fibroblasts.[9–11] However, a defect in LDLR internalization was observed in Epstein-Barr virus lymphocytes from ARH patients.[12] LDLR activity in these mutant cells could be restored by retrovirus-mediated expression of normal ARH.[13] The results indicated that lymphocytes require ARH for normal functioning of the LDLR even in vitro, whereas fibroblasts express the normal LDLR functions without ARH, at least in vitro. Because ARH patients have delayed clearance of LDL, the LDLR requires ARH for its functions, at least in the liver in vivo. Jones et al[14] reported that ARH-deficient mice have delayed catabolism of LDL, higher LDL cholesterol levels, and greater immunodetectable LDLR on the sinusoidal surface of hepatocytes.

In the present study, we characterized *ARH*-deficient mice to study the functions of ARH. *ARH*$^{-/-}$ mice showed a higher level of plasma LDL cholesterol than wild-type mice, whereas *ARH*$^{+/-}$ mice did not show hypercholesterolemia, being consistent with clinical manifestation of the human ARH patients.[5,7] The clearance of ^{125}I-LDL was delayed, and hepatic uptake of 1,1′-dioctadecyl-3,3,3′,3′-tetramethylindocarbocyanine perchlorate (DiI)-LDL and of [^{3}H]cholesteryl oleyl ether-labeled LDL (^{3}H-CE-LDL) was decreased in *ARH*$^{-/-}$ mice. However, primary cultured hepatocytes of *ARH*$^{-/-}$ mice had normal functions to internalize ^{3}H-CE-LDL, ^{125}I-LDL, and DiI-LDL. Thus, the results indicate that the cellular environment modulates the regulation of LDLR function by ARH protein.

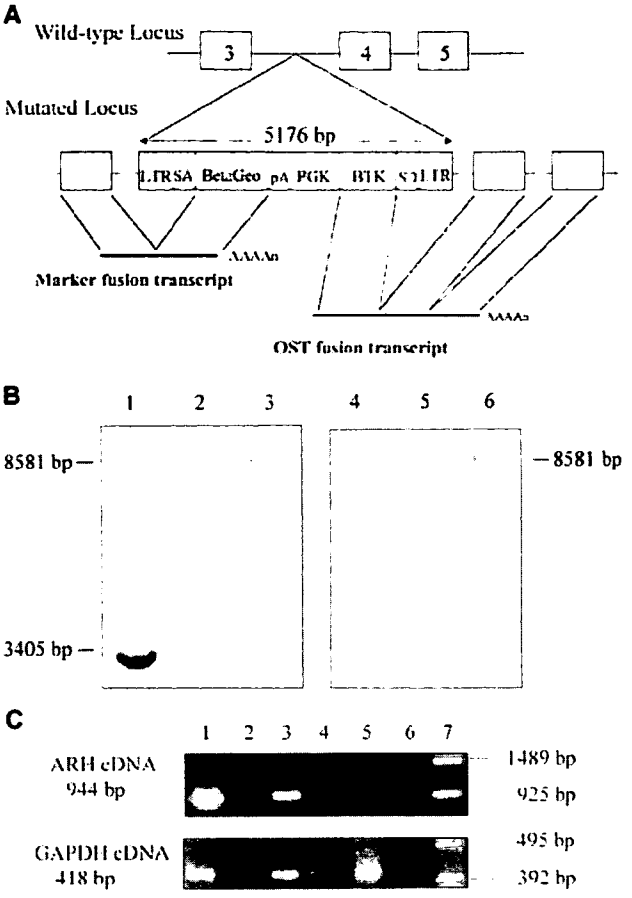

Figure 1. A, Strategy for insertional mutagenesis of the *ARH* locus in the mouse genome. The gene trap vector contains a promoterless splice acceptor sequence (SA) and BetaGeo, which create marker fusion transcripts. The vector also contains a long terminal repeat (LTR), a phosphoglycerate kinase-1 promoter (PGK), Bruton tyrosine kinase (BTK), and a splice donor sequence (SD). OmniBank Sequence Tag 149604 has an insertion of the vector in the third intron of *ARH* gene. B, Southern blot analysis of liver DNA. DNA was digested with *Apa*I and hybridized with a probe comprising portions of the mouse *ARH* gene containing exon 3 and intron 3 (lanes 1 to 3) or neo gene (lanes 4 to 6). Lanes 1 and 4, *ARH*$^{+/+}$; lanes 2 and 5, *ARH*$^{+/-}$; lanes 3 and 6, *ARH*$^{-/-}$. C, Reverse-transcription polymerase chain reaction of ARH and GAPDH mRNA. Lane 1 and 2, *ARH*$^{+/+}$; 3 and 4, *ARH*$^{+/-}$; 5 and 6, *ARH*$^{-/-}$. Lane 1, 3, and 5 are reverse-transcription plus; 2, 4, and 6 are reverse-transcription minus. Lane 7 shows size markers, lambda DNA digested with *Sty*1 for ARH, and phiX174 DNA digested with *Hin*cII for GAPDH.

Materials and Methods

General Procedure

Plasma lipoproteins were analyzed by high-performance liquid chromatography using molecular sieve columns (Skylight Biotech, Inc).[15] Cholesterol and triglycerides were measured using enzyme assay kits (Wako, Tokyo, Japan). Na^{125}I (37 GBq/mL) and [1α,2α(*n*)-^{3}H]cholesteryl oleyl ether (^{3}H-CE) (1.63 TBq/mmol) were purchased from Amersham (Buckinghamshire, UK). LDL was isolated by sequential ultracentrifugation in a density range of 1.019<density<1.064 from pooled plasma of apolipoprotein E knockout mice (Jackson Laboratory, Bar Harbor, Me) or normal human volunteers after overnight fasting. Human lipoprotein-deficient serum (LPDS) (density>1.215 g/mL) was prepared by ultracentrifugation.

Generation of Knockout Mouse

To generate *ARH* knockout mice, mutations were created by insertional mutagenesis using the gene trap vectors developed by Lexicon Genetics Incorporated (Woodlands, Tex), based on retroviral-based gene trap technology previously reported.[16] OmniBank Sequence Tag 149604 corresponded to the insertion mutation in the third intron of *ARH* gene in mouse chromosome 4 (Figure 1A). The line was obtained from Lexicon Genetics Incorporated. All experiments were performed with the F2-generation or F3-generation descendants, which were backcrossed with the C57Bl/6. LDLR knockout mice (*LDLR*$^{-/-}$) were generated as previously described,[17] which were backcrossed to C57Bl/6 mice, and were used for the study.

Southern Blot Analysis

Southern blot analysis was performed after digestion of the DNA prepared from liver with *Apa*I. ^{32}P-labeled polymerase chain reaction products (239 bp) amplified from portions of exon 3 and intron 3 of the mouse *ARH* gene with primers 5′-ATCATCCTGACCGACAGCCT-3′ and 5′-GGCACAACATAACCGACCTA-3′ or neo gene fragment (850 bp) derived from pBS64neo (Lexicon Genetics Inc) as probes according to the standard procedure.[18]

Reverse-Transcription Polymerase Chain Reaction

Total RNA was isolated from the liver of wild-type, heterozygous, and homozygous mice using the acid guanidium thiocyanate-phenol-chloroform method, as described.[19]

^{125}I-LDL Turnover Study

Mouse LDL was iodinated with ^{125}I by the iodine monochloride method[20] to give a specific activity of ^{125}I-LDL >200 cpm/ng

protein. Female mice of the genotypes of wild-type ($ARH^{+/+}$), $ARH^{+/-}$, $ARH^{-/-}$, and $LDLR^{-/-}$, 12 to 15 weeks of age, were fasted for 13 hours. Three mice in each genotype received an intravenous bolus via the external jugular vein of ^{125}I-labeled mouse LDL (5 μg of protein). Blood was collected from the tail vein with heparinized Pasteur pipette at the indicated timings. The plasma ^{125}I-labeled apoB was measured by isopropanol precipitation, followed by gamma counting as previously described.[17]

In Vivo Hepatic Uptake of Intravenously Injected DiI-LDL

Twelve-week-old female mice of the genotypes of wild-type, $ARH^{-/-}$, and $LDLR^{-/-}$ were fasted for 13 hours. Each mouse received an intravenous bolus via the external jugular vein of 50 μg of human DiI-LDL (Molecular Probes Inc, Eugene, Ore). To detect nonspecific incorporation of DiI-LDL, 2.5 mg of unlabeled human LDL was injected 2 minutes before 50 μg of DiI-LDL was injected. Two minutes after DiI-LDL injection, blood was collected for determination of cholesterol and lipoproteins. After 4 hours, the right atrium was punctured, 10 mL of phosphate-buffered saline (PBS) was injected via the left ventricle, and subsequently 10 mL of PBS containing 4% paraformaldehyde. The tissues were immersed in PBS containing 4% paraformaldehyde at 4°C for 12 hours. The liver samples were frozen in liquid nitrogen and subjected to microscopic analysis. To stain Kupffer cells, BM8 (rat antibody against mouse pan-macrophage) (BMA Biomedicals AG, Augst, Switzerland) was used as a primary antibody and fluorescein isothiocyanate-conjugated rabbit anti-rat IgG (DAKO Cytomation, Glostrup, Denmark) was used as a secondary antibody. The samples were observed by confocal laser scanning microscopy (LSM5 PASCAL; Zeiss, Co, Tokyo, Japan).

Labeling of Human LDL With ^{3}H-CE

LDL was labeled with ^{3}H-CE according to the previously described method,[21] with a minor modifications.

In Vivo Hepatic Uptake of Intravenously Injected ^{3}H-CE-LDL

^{3}H-CE-LDL (0.8 μCi) was injected via the external jugular vein of wild-type ($ARH^{+/+}$), $ARH^{-/-}$, and $LDLR^{-/-}$ female mice, 12 to 15 weeks of age. Blood was collected from the tail vein with heparinized Pasteur pipette at 2 minutes and 4 hours after the injection. The blood was dispersed in chloroform/methanol, 2/1 (v/v). Immediately after the second blood collection, 2 mg of human LDL was injected via the inferior vena cava. Ten minutes later, the right atrium was punctured and 20 mL of PBS was injected via the left ventricle three times to wash the blood from the body. The liver was isolated, immersed in chloroform/methanol 2/1 (v/v), and homogenized with a polytron homogenizer. The lipid was extracted from the liver and the blood by the method of Folch.[22] Radioactivity in each sample was counted in a liquid scintillation counter using a scintillation cocktail of toluene/Triton X100 (2:1) containing PPO (0.6%) and POPOP (0.05%).

Preparation and Culture of Mouse Hepatocytes

Mice (14 to 16 weeks of age) of the indicated genotype were used for the study. The livers were perfused via the portal vein and hepatocytes were obtained by the method of Seglen.[23] After 24-hour incubation in Waymouth MB 752/1 medium containing 10% fetal calf serum in six-well plates, the cells were subjected to the study.

In Vitro Uptake of ^{3}H-CE-LDL Into Primary Cultured Hepatocytes

The cells were incubated in Waymouth MB 752/1 medium containing 10% LPDS for 48 hours, and then incubated in DMEM containing 2% bovine serum albumin (without free fatty acid) and ^{3}H-CE-LDL (5 to 100 μg/mL) for an additional 3 hours. Then, the cells were washed twice with 150 mmol/L NaCl, 50 mmol/L of Tris-HCl (pH 7.4) containing 2 mg/mL of bovine serum albumin, and once with the same buffer without bovine serum albumin. The cells were incubated with LDL-releasing buffer (50 mmol/L NaCl, 10 mmol/L Hepes (pH 7.4), containing 10 mg/mL heparin) at 4°C for 1 hour. After removal of the heparin-releasable fraction, 1 mL of hexane/isopropyl alcohol (3/2) was added to the cells to extract lipids in the cells.[24] After delipidation, the cells were dissolved in 1 N NaOH and protein concentration was measured.

^{125}I-LDL Binding, Incorporation, and Degradation Assays

Waymouth MB 752/1 medium containing 10% LPDS was added to the cells and incubated for another 24 hours. Binding, internalization, and degradation of ^{125}I-LDL were analyzed according to the method previously described.[25]

DiI-LDL Incorporation Into Primary Cultured Hepatocytes

The cells were added to Waymouth MB 752/1 medium containing 10% LPDS and incubated for 24 hours. Then, the cells were washed twice and incubated at 37°C for 3 hours with 50 μg/mL of DiI-LDL in 0.2 mL of MEM containing 10% LPDS. Nonspecific incorporation was determined by parallel incubation in the presence of 20-fold excess of LDL. The cells were washed three times with PBS containing 0.2% bovine serum albumin, followed by washing twice with PBS. The samples were observed with a laser confocal microscopy.

An expanded Materials and Methods section is available in the online data supplement at http://circres.ahajournals.org.

Results

Generation of *ARH* Knockout Mice

OmniBank Sequence Tag 149604 (Lexicon Genetics Inc) corresponded to the insertion mutation in the third intron of *ARH* gene in mouse chromosome 4 (Figure 1A). The mutated allele encodes a marker fusion transcript and OmniBank Sequence Tag fusion transcript instead of *ARH* mRNA. The offspring heterozygous animals were mated to produce $ARH^{+/+}$, $ARH^{+/-}$, and $ARH^{-/-}$ mice. Southern blot analysis was performed to genotype the mice using a probe comprising portions of mouse *ARH* gene containing both exon 3 and intron 3 (Figure 1B) after digestion of DNA with *Apa*I. *Apa*I site is not present in the insertion fragment used for development of the knockout mice. Southern blot analysis with the exon probe showed a 3405-bp band for the wild-type allele and was observed in both the wild-type and $ARH^{+/-}$ mice, whereas an 8581-bp band, the disrupted allele which was produced by the insertion of 5176-bp fragment (Figure 1A), was observed in $ARH^{+/-}$ and $ARH^{-/-}$ mice after digestion of DNA with *Apa*I. Southern blot analysis with neo gene probe demonstrated that only one position and one copy insertion event occurred in a mouse genome because $ARH^{+/-}$ and $ARH^{-/-}$ exhibited an 8581 bp.

To confirm that the mutated allele does not express the mRNA, total RNA was isolated from the livers of the animals of each genotype and analyzed by reverse-transcription polymerase chain reaction (Figure 1C). A 944-bp band, the *ARH* transcript that was expressed in wild-type and $ARH^{+/-}$mice, was not detectable in $ARH^{-/-}$ mice. The results thus confirmed that the insertion mutation by gene trap vector disrupted the *ARH* gene expression.

TABLE 1. Lipid and Lipoprotein Profiles of ARH Knockout Mice (mean±SEM)

	Total Cholesterol, mmol/L	Triglyceride, mmol/L	HDL Cholesterol, mmol/L	LDL Cholesterol, mmol/L
Wild type				
Male (n=5)	2.68±0.14	1.04±0.26	2.49±0.12	0.17±0.05
Female (n=8)	2.57±0.22	0.78±0.07	2.20±0.19	0.30±0.04
Heterozygote				
Male (n=8)	2.92±0.14	1.00±0.13	2.78±0.11	0.13±0.03
Female (n=10)	2.82±0.19	0.76±0.06	2.40±0.14	0.35±0.08
Homozygote				
Male (n=5)	4.53±0.35†	1.20±0.10	3.10±0.52	1.01±0.21†
Female (n=8)	4.64±0.68†	1.09±0.19	2.96±0.30*	1.46±0.44*

*$P<0.05$.
†$P<0.01$ vs wild type.

Lipid and Lipoprotein Profiles of *ARH* Knockout Mice

Table 1 shows total plasma cholesterol, triglycerides, LDL cholesterol, and HDL cholesterol levels of mice from litters derived from the mating of $ARH^{+/-}$ mice fed a normal chow. Plasma total cholesterol levels were 1.8-fold higher in $ARH^{-/-}$ mice than those in $ARH^{+/+}$. The elevation of total cholesterol was attributed to the six-fold increase of LDL cholesterol. There was no significant difference in the plasma cholesterol levels between $ARH^{+/-}$ and $ARH^{+/+}$ mice. Histological analysis of the liver showed that $ARH^{-/-}$ mice at 12 weeks of age did not have fatty livers, which were observed in our ARH patients.[5]

^{125}I-LDL Turnover Study

To investigate the LDL metabolism in ARH deficiency, ^{125}I-LDL turnover study was performed in $ARH^{-/-}$, $ARH^{+/-}$, $ARH^{+/+}$ (wild-type), and $LDLR^{-/-}$ mice. The clearance of ^{125}I-LDL from circulation is demonstrated in a semilogarithmic plot in Figure 2. It was substantially retarded in $ARH^{-/-}$ and $LDLR^{-/-}$ mice compared with wild-type mice. The clearance rate of ^{125}I-LDL in $ARH^{+/-}$ mice was similar to that in wild-type mice. The half-lives of the plasma ^{125}I-LDL were 11.7 hours in $ARH^{-/-}$ and 6.0 hours in $LDLR^{-/-}$ mice, and both were longer than those in $ARH^{+/-}$ and wild-type mice (2.8 hours).

Microscopic Findings in the Liver After Injection of DiI-LDL

To study whether the delayed clearance of LDL in $ARH^{-/-}$ mice is attributable to impaired catabolism of LDL in the liver, the liver specimen was examined after injection of DiI-LDL in wild-type, $LDLR^{-/-}$, and $ARH^{-/-}$ mice (Figure 3). Kupffer cells were identified by fluorescein isothiocyanate (Figure 3B, 3D, 3F, 3H, 3J, and 3L). Fluorescence activity was detected in the cytosol of the hepatocytes and Kupffer cells in wild-type mice, indicating that both types of cells effectively take-up DiI-LDL (Figure 3A). Pre-injection of 2.5 mg LDL raised serum total cholesterol from 2.18±0.66 (mean±SD) mmol/L to 14.67±0.68 mmol/L, and LDL cholesterol from 0.21±0.07 mmol/L to 11.42±1.09 mmol/L in wild-type mice (Table 2). In this condition, the incorporation

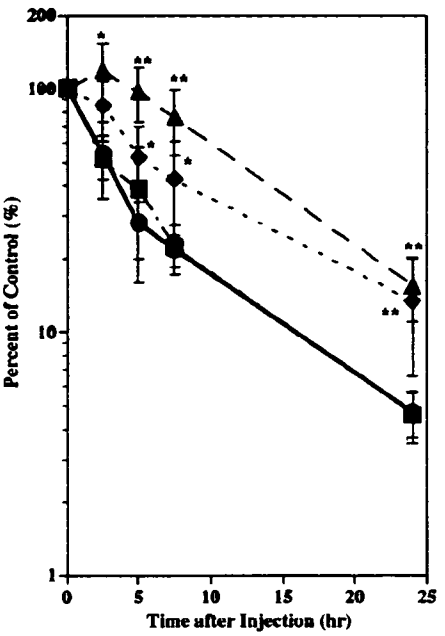

Figure 2. ^{125}I-LDL turnover study of wild-type (●), $ARH^{+/-}$ (■), $ARH^{-/-}$ (▲), and $LDLR^{-/-}$ (♦) mice. After 13 hours of fasting, wild-type, $ARH^{+/-}$, $ARH^{-/-}$, and $LDLR^{-/-}$ mice (three of each) were injected with 5 μg of ^{125}I-LDL. After the indicated time, blood was collected from the tail vein. The plasma content of ^{125}I-labeled apoB was measured by isopropanol precipitation, followed by gamma counting. The data are shown in semilogarithmic plots, and each data point represents the mean±SEM for triplicate assay. *$P<0.05$, **$P<0.01$.

of DiI-LDL into hepatocytes was decreased by the excess amount of LDL in plasma (Figure 3C), whereas its incorporation into Kupffer cells was not affected. In contrast, hepatocytes of $ARH^{-/-}$ mice were stained less extensively than those of wild-type mice by DiI-LDL fluorescence (Figure 3I), indicating that the uptake of DiI-LDL by the hepatocytes of $ARH^{-/-}$ mice was smaller than that of wild-type mice, and the presence of excess amount of LDL in plasma did not influence this result (Figure 3K). The fluorescence in the hepatocytes of $LDLR^{-/-}$ mice was also less intense than that in $ARH^{-/-}$ (Figure 3E).

In Vivo Hepatic Uptake of Intravenously Injected ^{3}H-CE-LDL

Hepatic uptake of LDL was also investigated by injecting ^{3}H-CE-LDL. Four hours after the injection, the tritium count in the blood decreased by 44% in wild-type mice, whereas it did not decrease in either $LDLR^{-/-}$ or $ARH^{-/-}$ mice (Figure 4A). The liver of wild-type mice incorporated 27.4±8.0% (mean±SD) of the injected ^{3}H-CE-LDL, whereas 9.0±1.0% was incorporated in $LDLR^{-/-}$ mice and 11.8±0.5% in $ARH^{-/-}$ mice (Figure 4B). The amount of ^{3}H-CE-LDL taken-up by the liver in $ARH^{-/-}$ was significantly smaller than that in wild-type mice but larger than that in $LDLR^{-/-}$ mice ($P<0.05$).

Incorporation of LDL in Primary Cultured Hepatocytes

In an attempt to reproduce the in vivo observations in vitro, incorporation of ^{3}H-CE-LDL was examined in primary cul-

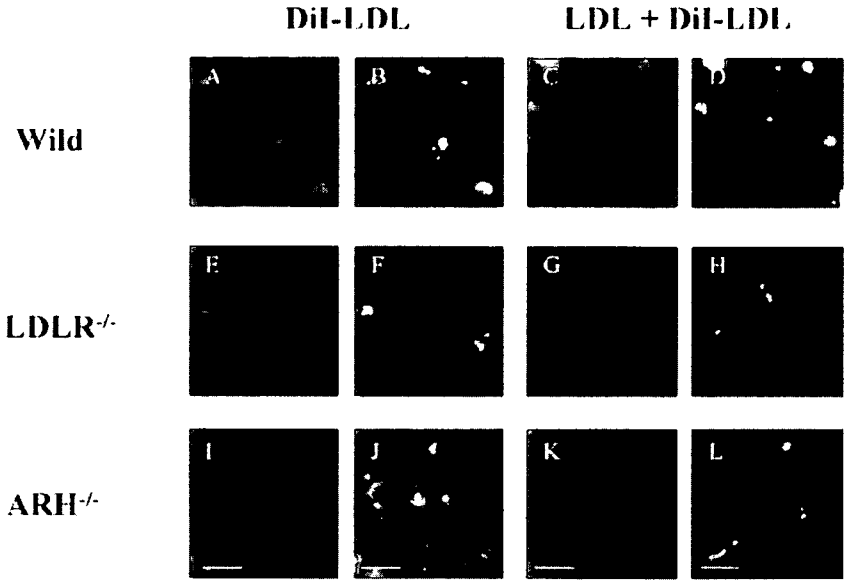

Figure 3. Microscopic findings of the liver after injection of DiI-LDL. A, E, and I, The liver from a mouse of each genotype 4 hours after the injection of 50 μg of DiI-LDL. C, G, and K, The liver from a mouse of each genotype, 4 hours after the injection of 2.5 mg of LDL, followed by 50 μg of DiI-LDL. B, F, and J, The liver from a mouse of each genotype, 4 hours after the injection of 50 μg of DiI-LDL. The specimens were stained with rat anti-mouse pan-macrophage antibody. D, H, and L, The liver from each genotype of mouse 4 hours after injection of 2.5 mg of LDL, followed by 50 μg of DiI-LDL. The specimen was stained with rat anti-mouse pan-macrophage antibody. The scale bar indicates 20 μm.

tured hepatocytes. Interestingly, the hepatocytes of *ARH*$^{-/-}$ mice internalized ^{3}H-CE-LDL as much as those of wild-type mice, whereas the hepatocytes of *LDLR*$^{-/-}$ mice took-up significantly less ^{3}H-CE-LDL (Figure 5A). The cultured hepatocytes of *ARH*$^{-/-}$ mice bound larger amounts of ^{125}I-LDL than those of wild-type and *LDLR*$^{-/-}$ mice. The hepatocytes of *ARH*$^{-/-}$ internalized and degraded ^{125}I-LDL as much as those of wild-type mice, which was significantly more than those of *LDLR*$^{-/-}$ mice (Figure 5B through 5D).

DiI-LDL Incorporation in Primary Cultured Hepatocytes

To confirm the positive incorporation of LDL by the primary cultured hepatocytes without ARH, the hepatocytes of *ARH*$^{-/-}$, *LDLR*$^{-/-}$, and wild-type mice were incubated with DiI-LDL and were observed by a laser confocal microscopy. Fluorescence-positive substances were observed in the cytosol of the hepatocytes of wild-type mice (Figure 6A), and they were suppressed in the presence of excess amounts of LDL (Figure 6B). The cultured hepatocytes of *LDLR*$^{-/-}$ mice showed very low fluorescence activity (Figure 6C and 6D). In contrast, the hepatocytes of *ARH*$^{-/-}$ mice showed fluorescence uptake of amounts similar to those observed for the wild-type (Figure 6E), and this was efficiently suppressed by excess amounts of LDL (Figure 6F).

TABLE 2. Cholesterol Levels of Total, VLDL, LDL, and HDL Fractions Before and After Administration of 2.5 mg LDL

	Total Cholesterol, mmol/L		VLDL Cholesterol, mmol/L		LDL Cholesterol, mmol/L		HDL Cholesterol, mmol/L	
	Before	After	Before	After	Before	After	Before	After
Wild-1	2.36	14.30	0.02	1.99	0.12	10.56	2.22	1.74
Wild-2	2.72	14.27	0.05	1.37	0.24	11.04	2.44	1.86
Wild-3	1.45	15.45	0.06	2.10	0.26	12.64	1.13	0.71
Mean	2.18	14.67	0.04	1.82	0.21	11.42	1.93	1.43
SD	0.66	0.68	0.02	0.39	0.07	1.09	0.70	0.63

VLDL indicates very-low-density lipoprotein.

Discussion

ARH knockout mice were developed by insertion mutation in the third intron of mouse chromosome 4. *ARH*$^{-/-}$ mice had a 1.8-fold higher plasma total cholesterol than wild-type litter mates fed normal chow, and this was attributed to a six-fold increase of LDL. Total cholesterol levels in *ARH*$^{-/-}$ mice (Table 1) were slightly lower than those reported for *LDLR*$^{-/-}$ mice (5.90±0.23 mmol/L in male, 6.18±0.21 mmol/L in female),[17] and cholesterol levels in *ARH*$^{+/-}$ mice (2.92±0.14 mmol/L in male, 2.82±0.19 mmol/L in female) were almost the same as those in *ARH*$^{+/+}$ mice (2.68±0.14 mmol/L in male, 2.57±0.22 mmol/L in female). The hypercholesterolemia in our *ARH*$^{-/-}$ mice appears to be milder than that reported by Jones et al,[14] who have recently reported that total cholesterol levels were moderately higher both in *ARH*$^{-/-}$ mice (7.96±1.63 mmol/L) and in *ARH*$^{+/-}$ mice (4.06±0.58 mmol/L) compared with that in *ARH*$^{+/+}$ mice (3.26±1.00 mmol/L) fed a chow containing 0.2% cholesterol. The difference in the plasma total cholesterol values between our *ARH*$^{-/-}$ mice and theirs may stem from different cholesterol content of the diet, because the chow we used contained 0.1% cholesterol.

The clearance of ^{125}I-LDL from the circulation was significantly delayed in *ARH*$^{-/-}$ mice like in *LDLR*$^{-/-}$ mice (Figure 2), indicating that the in vivo catabolic rate of LDL is decreased in *ARH*$^{-/-}$ mice. The half-life for the disappearance of ^{125}I-LDL in *ARH*$^{-/-}$ mice (11.7 hours) was longer than that observed in wild-type mice (2.8 hours) but not significantly different from that in *LDLR*$^{-/-}$ (6.0 hours). The LDL clearance in *ARH*$^{+/-}$ mice was same as that in the wild-type mice, suggesting that their LDL catabolism is normal. These results appear to be consistent with the findings in the ARH patients.[5]

To investigate the in vivo mechanism for the delayed catabolism of LDL directly in *ARH*$^{-/-}$ mice, hepatic uptake of

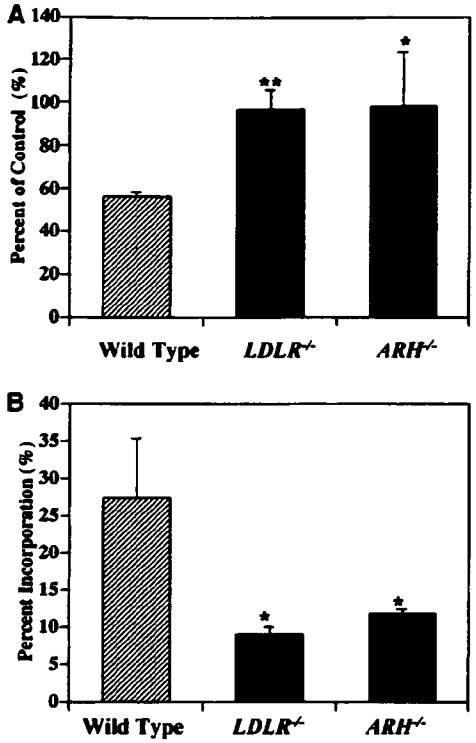

Figure 4. Hepatic uptake of intravenously injected ^{3}H-CE-LDL. ^{3}H-CE-LDL was injected into a mouse of each genotype. The blood was collected at 2 minutes and 4 hours after the injection. Immediately after the blood collection at 4 hours, 2 mg of LDL was injected and equilibrated for 10 minutes. The blood was washed from the body as described in the Methods section, and the liver was isolated. Lipid was extracted from the liver and the blood, and radioactivity was counted. Values are mean±SEM. A, Percentage of remaining tritium radioactivity in the mouse blood after 4 hours compared to that after 2 minutes. B, Hepatic uptake of tritium in the liver, 4 hours after injection, expressed as percentage of the total radioactivity injected calculated from the count in the blood at 2 minutes after the injection. $^{*}P<0.05$, $^{**}P<0.01$.

DiI-LDL was monitored. The fluorescence was recovered in the cytosols of both hepatocytes and Kupffer cells of wild-type mice (Figure 3A), and the fluorescence in the hepatocytes was suppressed by pretreatment with excess amounts of LDL (Figure 3C), suggesting that DiI-LDL was incorporated into the hepatocytes via the LDLR. Lower levels of DiI-LDL were found in hepatocytes of *LDLR*$^{-/-}$ and *ARH*$^{-/-}$ mice (Figure 3E, I). Because LDL cholesterol levels were higher in *ARH*$^{-/-}$ mice (1.01±0.21 mmol/L in male, 1.46±0.44 mmol/L in female) than that in wild-type mice (0.17±0.05 mmol/L in male, 0.30±0.04 mmol/L in female), injected DiI-LDL may become more diluted in *ARH*$^{-/-}$ by their own LDL. However, hepatic DiI-LDL uptake in *ARH*$^{-/-}$ mice was much lower than the observed uptake in wild-type mice when the excess LDL was given to raise LDL cholesterol (11.42±1.09 mmol/L). This indicates that the lower uptake of DiI-LDL in *ARH*$^{-/-}$ was not attributable to a dilution effect caused by their high LDL levels (Figure 3C, I).

Small numbers of cells appeared highly fluorescence-positive in the liver of mice of all the genotypes including *LDLR*$^{-/-}$ (Figure 3A, E, I). Their fluorescent activity was not

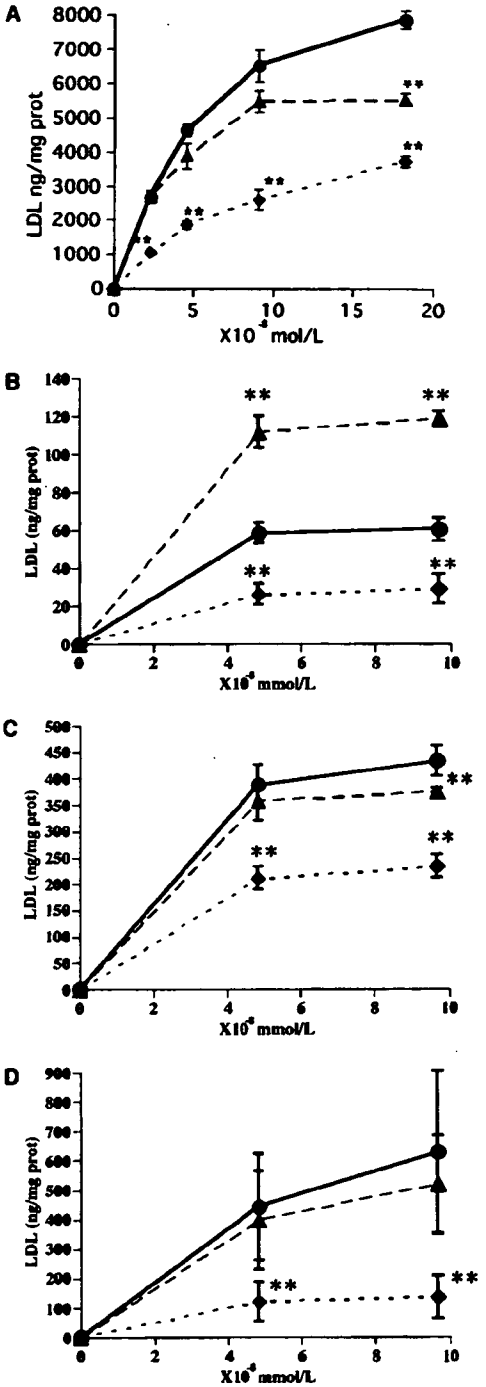

Figure 5. LDL receptor assay in primary cultured hepatocytes. Hepatocytes were obtained from the wild-type, *ARH*$^{-/-}$, and *LDLR*$^{-/-}$ mice, and cultured in Waymouth medium containing 10% fetal calf serum (day 0). On day 2, the medium was removed and the cells were washed twice. Then, the cells were cultured in Waymouth medium containing 10% LPDS. On day 3, the cells were subjected to LDL receptor assay. The data are shown as the mean±SEM of quadruplicate assays. The experiments were performed in the presence of 20-fold excess of LDL for nonspecific binding. A, ^{3}H-CE-LDL incorporation of primary cultured hepatocytes from wild-type (●), *LDLR*$^{-/-}$ (♦), and *ARH*$^{-/-}$ (▲) mice. $^{*}P<0.05$, $^{**}P<0.01$ vs wild-type. B, ^{125}I-LDL binding of primary cultured hepatocytes. C, ^{125}I-LDL incorporation of primary cultured hepatocytes. D, ^{125}I-LDL degradation of primary cultured hepatocytes.

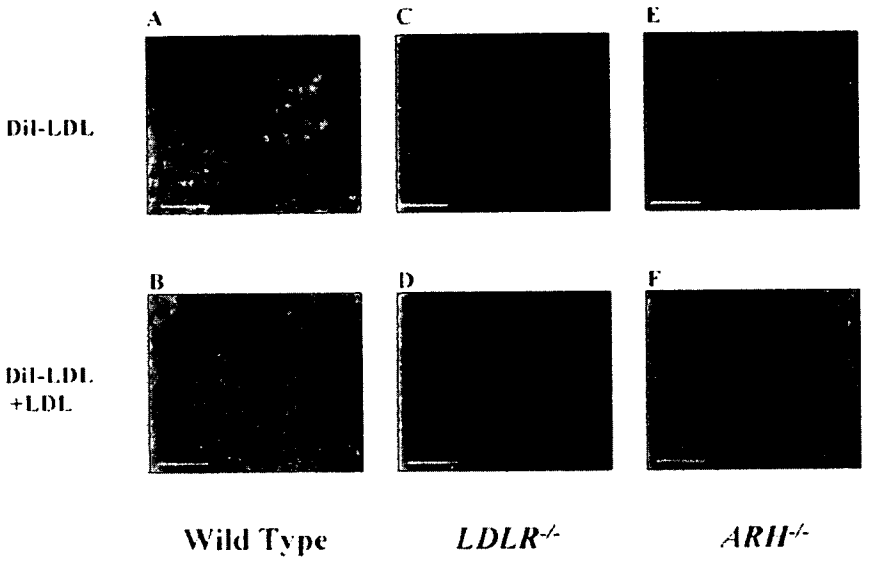

Figure 6. Dil-LDL incorporation in primary cultured hepatocytes of wild-type, $LDLR^{-/-}$, and $ARH^{-/-}$ mice. On day 0, hepatocytes were obtained from wild-type, $ARH^{-/-}$, and $LDLR^{-/-}$ mice, and cultured in Waymouth medium containing 10% fetal calf serum. After 4 hours, the cells were washed with PBS and cultured in Waymouth medium containing 10% LPDS. On day 2, the cells were incubated with Dil-LDL with or without 20 times excess of LDL for 3 hours. Then the cells were washed with PBS and mounted. A, C, and E, Hepatocytes from each genotype of mouse incubated with Dil-LDL. B, D, and F, Hepatocytes from each genotype of mouse incubated with Dil-LDL and excess of LDL. The scale bar indicates 10 μm.

decreased by the presence of excess amounts of LDL (Figure 3C, G, K) and these cells were positively identified as Kupffer cells by immunostaining with the antibody against mouse macrophages (Figure 3B, D, F, H, J, L). Thus, DiI-LDL was incorporated into Kupffer cells via an LDLR-independent pathway.

Hepatic uptake of LDL in $ARH^{-/-}$ was also examined by measuring the uptake of ^{3}H-CE-LDL by the liver. The tritium count in the blood decreased significantly in the wild-type mice, whereas it did not change in $LDLR^{-/-}$ and $ARH^{-/-}$ mice (Figure 4A). This is in agreement with the ^{125}I-LDL turnover study (Figure 2). The incorporation of ^{3}H-CE-LDL into the liver of $LDLR^{-/-}$ and $ARH^{-/-}$ mice was significantly lower than that of the wild-type mice (Figure 4B), suggesting again that the delayed turnover of LDL in $ARH^{-/-}$ mice is attributable to low LDL uptake by the liver. Interestingly, incorporation of ^{3}H-CE-LDL into the liver of $ARH^{-/-}$ is significantly higher than that of $LDLR^{-/-}$ ($P<0.05$). This result implies that the LDLR may function to incorporate LDL in the liver to some extent in vivo even without ARH.

To examine in vitro LDLR activity in the cells of $ARH^{-/-}$ mice, the incorporation of ^{3}H-CE-LDL was measured in primary cultured hepatocytes of $ARH^{-/-}$, $LDLR^{-/-}$, and wild-type mice (Figure 5A). The cultured hepatocytes of $ARH^{-/-}$ incorporated a slightly smaller amount of ^{3}H-CE-LDL than that of the wild-type, but much larger than that of $LDLR^{-/-}$. These findings were confirmed by ^{125}I-LDL incorporation and degradation experiments (Figure 5C, D). The binding of ^{125}I-LDL to the hepatocytes of $ARH^{-/-}$ was larger than that of wild-type (Figure 5B). Recently, Michaely et al[26] reported that the number of LDLRs on the cell surface of the lymphocytes in ARH subject was increased 20-fold, and that LDL binding activity was increased two-fold. The hepatocytes of $ARH^{-/-}$ seemed to remain the characteristics of in vivo status to some extent. To see whether LDL is incorporated into the cell or whether it remains on the cell surface, the cells were incubated with DiI-LDL and observed by using a laser confocal microscopy. The cytosol of the hepatocytes of $ARH^{-/-}$ mice was fluorescently stained, suggesting that DiI-LDL was internalized, like that of wild-type mice (Figure 6A, E). The results were highly consistent with the findings that the LDLR in the cultured fibroblasts from the homozygous ARH patients normally functioned, despite the fact that LDL clearance in their blood was severely impaired.[5] This suggests that the LDLR functions normally in vitro without ARH protein.

The PTB domain of ARH protein has been shown, by pull-down technique, to bind to the FDNPVY sequence of the LDLR protein.[8] ARH protein was also reported to interact with clathrin and AP-2, and it is suggested to function as an adaptor protein that couples LDLR to the endocytic machinery. ARH patients have severe hypercholesterolemia caused by delayed LDL clearance in vivo, although they have normal or subnormal levels of LDLR activity in their fibroblasts when measured in vitro.[5] However, transformed lymphocytes and monocyte-derived macrophages were unable to internalize LDL in ARH patients.[12] Thus, the dependency of LDLR function on ARH protein can be cell-specific. However, we have demonstrated here that hepatocytes do not take-up LDL in vivo without ARH protein, but they normally catabolize LDL in vitro. Thus, the requirement of ARH protein for proper functioning of the LDLR is not cell-specific, but rather may depend on the cellular environment.

Hepatic uptake of ^{3}H-CE from LDL was shown to be significantly higher in $ARH^{-/-}$ mice than $LDLR^{-/-}$ mice. This may indicate that LDLR functions to some extent without ARH, even in vivo. Some other adaptor proteins may compensate for ARH by forming an LDLR–clathrin complex, or the condition can be induced so LDLRs can be internalized without forming a clathrin complex. Our in vitro results strongly indicate that these possibilities may be enabled in a certain cellular environments.

Acknowledgments

This work was supported in part by the Promotion of Fundamental Studies in Health Science of the Organization for Pharmaceutical Safety and Research (OPSR); Research on Advanced Medical Technology from the Ministry of Health, Labour, and Welfare; Ono Medical Research Foundation; Takeda Medical Research Founda-

tion; and grant-in-aid for Scientific Research (C) (No. 15590964) from the Ministry of Education, Science, Sports, and Culture, Japan. We thank Drs Kenji Kangawa, Hisayuki Matsuo, and Hitonobu Tomoike for their helpful discussion and advice, Dr Michitaka Masuda for taking the photograph, and Dr Patrick Leahy for proofreading this manuscript. We also thank Moto Ohira, Eri Abe, Ritsuko Maeda, and Keiko Jinno for their excellent technical assistance.

References

1. Khachadurian AK, Uthman SM. Experiences with the homozygous cases of familial hypercholesterolemia. A report of 52 patients. *Nutr Metab.* 1973;15:132–140.
2. Brown MS, Anderson RG, Basu SK, Goldstein JL. Recycling of cell-surface receptors: observations from the LDL receptor system. *Cold Spring Harb Symp Quant Biol.* 1982;46(Pt 2):713–721.
3. Goldstein JL, Hobbs HH, Brown MS. Familial hypercholesterolemia. In: Scriver CR, Beaudet AL, Sly WS, Valle D, eds. *The Metabolic and Molecular Bases of Inherited Disease.* 8th ed., Vol II. New York: McGraw-Hill; 2001;2863–2913.
4. Harada-Shiba M, Tajima S, Miyake Y, Kojima S, Tsushima M, Yamamoto A. Severe hypercholesterolemia patients with normal LDL receptor. *J Jpn Atheroscler Soc.* 1991;19:227–242.
5. Harada-Shiba M, Tajima S, Yokoyama S, Miyake Y, Kojima S, Tsushima M, Kawakami M, Yamamoto A. Siblings with normal LDL receptor activity and severe hypercholesterolemia. *Arterioscler Thromb.* 1992;12:1071–1078.
6. Garcia CK, Wilund K, Arca M, Zuliani G, Fellin R, Maioli M, Calandra S, Bertolini S, Cossu F, Grishin N, Barnes R, Cohen JC, Hobbs HH. Autosomal recessive hypercholesterolemia caused by mutations in a putative LDLR adaptor protein. *Science.* 2001;292:1394–1398.
7. Harada-Shiba M, Takagi A, Miyamoto Y, Tsushima M, Ikeda Y, Yokoyama S, Yamamoto A. Clinical features and genetic analysis of autosomal recessive hypercholesterolemia. *J Clin Endocrinol Metab.* 2003;88:2541–2547.
8. He G, Gupta S, Yi M, Michaely P, Hobbs HH, Cohen JC. ARH is a modular adaptor protein that interacts with the LDL receptor, clathrin, and AP-2. *J Biol Chem.* 2002;277:44044–44049.
9. Schmidt HH, Stuhrmann M, Shamburek R, Schewe CK, Ebhardt M, Zech LA, Buttner C, Wendt M, Beisiegel U, Brewer HB, Jr, Manns MP. Delayed low density lipoprotein (LDL) catabolism despite a functional intact LDL-apolipoprotein B particle and LDL-receptor in a subject with clinical homozygous familial hypercholesterolemia. *J Clin Endocrinol Metab.* 1998;83:2167–2174.
10. Zuliani G, Arca M, Signore A, Bader G, Fazio S, Chianelli M, Bellosta S, Campagna F, Montali A, Maioli M, Pacifico A, Ricci G, Fellin R. Characterization of a new form of inherited hypercholesterolemia: familial recessive hypercholesterolemia. *Arterioscler Thromb Vasc Biol.* 1999;19:802–809.
11. Zuliani G, Vigna GB, Corsini A, Maioli M, Romagnoni F, Fellin R. Severe hypercholesterolaemia: unusual inheritance in an Italian pedigree. *Eur J Clin Invest.* 1995;25:322–331.
12. Norman D, Sun XM, Bourbon M, Knight BL, Naoumova RP, Soutar AK. Characterization of a novel cellular defect in patients with phenotypic homozygous familial hypercholesterolemia. *J Clin Invest.* 1999;104:619–628.
13. Eden ER, Patel DD, Sun XM, Burden JJ, Themis M, Edwards M, Lee P, Neuwirth C, Naoumova RP, Soutar AK. Restoration of LDL receptor function in cells from patients with autosomal recessive hypercholesterolemia by retroviral expression of ARH1. *J Clin Invest.* 2002;110:1695–1702.
14. Jones C, Hammer RE, Li WP, Cohen JC, Hobbs HH, Herz J. Normal sorting but defective endocytosis of the low density lipoprotein receptor in mice with autosomal recessive hypercholesterolemia. *J Biol Chem.* 2003;278:29024–29030.
15. Usui S, Hara Y, Hosaki S, Okazaki M. A new on-line dual enzymatic method for simultaneous quantification of cholesterol and triglycerides in lipoproteins by HPLC. *J Lipid Res.* 2002;43:805–814.
16. Zambrowicz BP, Friedrich GA, Buxton EC, Lilleberg SL, Person C, Sands AT. Disruption and sequence identification of 2,000 genes in mouse embryonic stem cells. *Nature.* 1998;392:608–611.
17. Ishibashi S, Brown MS, Goldstein JL, Gerard RD, Hammer RE, Herz J. Hypercholesterolemia in low density lipoprotein receptor knockout mice and its reversal by adenovirus-mediated gene delivery. *J Clin Invest.* 1993;92:883–893.
18. Sambrook J, Russell DW. *Molecular Cloning: A Laboratory Manual.* Cold Spring Harbor: Cold Spring Harbor Laboratory Press; 2001.
19. Nishimura N, Harada-Shiba M, Tajima S, Sugano R, Yamamura T, Qiang QZ, Yamamoto A. Acquisition of secretion of transforming growth factor-beta 1 leads to autonomous suppression of scavenger receptor activity in a monocyte-macrophage cell line, THP-1. *J Biol Chem.* 1998;273:1562–1567.
20. Bilheimer DW, Eisenberg S, Levy RI. The metabolism of very low density lipoprotein proteins. I. Preliminary in vitro and in vivo observations. *Biochim Biophys Acta.* 1972;260:212–221.
21. Nishikawa O, Yokoyama S, Okabe H, Yamamoto A. Enhancement of non-polar lipid transfer reaction through stabilization of substrate lipid particles with apolipoproteins. *J Biochem (Tokyo).* 1988;103:188–194.
22. Folch J, Lees M, Sloane Stanley GH. A simple method for the isolation and purification of total lipides from animal tissues. *J Biol Chem.* 1957;226:497–509.
23. Seglen PO. Control of glycogen metabolism in isolated rat liver cells by glucose, insulin and glucagon. *Acta Endocrinol Suppl (Copenh).* 1974;191:153–158.
24. Hara H, Yokoyama S. Interaction of free apolipoproteins with macrophages. Formation of high density lipoprotein-like lipoproteins and reduction of cellular cholesterol. *J Biol Chem.* 1991;266:3080–3086.
25. Goldstein JL, Basu SK, Brown MS. Receptor-mediated endocytosis of low-density lipoprotein in cultured cells. *Methods Enzymol.* 1983;98:241–260.
26. Michaely P, Li WP, Anderson RG, Cohen JC, Hobbs HH. The modular adaptor protein ARH is required for low density lipoprotein (LDL) binding and internalization but not for LDL receptor clustering in coated pits. *J Biol Chem.* 2004;279:34023–34031.

THE JOURNAL OF BIOLOGICAL CHEMISTRY
Vol. 279, No. 30, Issue of July 23, pp. 30938–30944, 2004
Printed in U.S.A.

Scavenger Receptor Expressed by Endothelial Cells I (SREC-I) Mediates the Uptake of Acetylated Low Density Lipoproteins by Macrophages Stimulated with Lipopolysaccharide*

Received for publication, December 1, 2003, and in revised form, May 11, 2004
Published, JBC Papers in Press, May 15, 2004, DOI 10.1074/jbc.M313088200

Yoshiaki Tamura‡, Jun-ichi Osuga‡, Hideki Adachi§, Ryu-ichi Tozawa‡, Yasukazu Takanezawa¶, Ken Ohashi‡, Naoya Yahagi‡, Motohiro Sekiya‡, Hiroaki Okazaki‡, Sachiko Tomita‡, Yoko Iizuka‡, Hiroyuki Koizumi¶, Toshihiro Inaba‖, Hiroaki Yagyu‖, Nobuo Kamada, Hiroshi Suzuki‡‡, Hitoshi Shimano§§, Takashi Kadowaki‡, Masafumi Tsujimoto§, Hiroyuki Arai¶, Nobuhiro Yamada§§, and Shun Ishibashi‡‖¶¶**

*From the ‡Department of Metabolic Diseases, Faculty of Medicine, University of Tokyo 7-3-1 Hongo, Bunkyo-ku, Tokyo 113-8655, Japan, the §Laboratory of Cellular Biochemistry, Institute of Physical and Chemical Research (RIKEN), Wako-shi, Saitama 351-0198, Japan, the ¶Department of Health Chemistry, Graduate School of Pharmaceutical Science, University of Tokyo 7-3-1 Hongo, Bunkyo-ku, Tokyo 113-0033, Japan, the ‖Department of Internal Medicine, Jichi Medical School, 3311-1 Yakushiji, Minamikawachi-machi, Kawachi-gun, Tochigi 329-0498, Japan, the **Chugai Research Institute for Medical Science Incorporated, 1-135 Komakado, Gotenba, Shizuoka 412-8513, Japan, the ‡‡Unit for Functional Genomics, National Research Center for Protozoan Diseases, Obihiro University of Agriculture and Veterinary Medicine, Nishi-2, Inada, Obihiro, Hokkaido 080-8555, Japan, and §§Metabolism, Endocrinology, and Atherosclerosis, Institute of Clinical Medicine, University of Tsukuba, 1-1-1 Tennodai, Tsukuba, Ibaraki 305-8575, Japan*

Scavenger receptor expressed by endothelial cells I (SREC-I) is a novel endocytic receptor for acetylated low density lipoprotein (LDL). Here we show that SREC-I is expressed in a wide variety of tissues, including macrophages and aortas. Lipopolysaccharide (LPS) robustly stimulated the expression of SREC-I in macrophages. In an initial attempt to clarify the role of SREC-I in the uptake of modified lipoproteins as well as in the development of atherosclerosis, we generated mice with a targeted disruption of the *SREC-I* gene by homologous recombination in embryonic stem cells. To exclude the overwhelming effect of the type A scavenger receptor (SR-A) on the uptake of Ac-LDL, we further generated mice lacking both SR-A and SREC-I (*SR-A*$^{-/-}$;*SREC-I*$^{-/-}$) by cross-breeding and compared the uptake and degradation of Ac-LDL in the isolated macrophages. The contribution of SR-A and SREC-I to the overall degradation of Ac-LDL was 85 and 5%, respectively, in a non-stimulated condition. LPS increased the uptake and degradation of Ac-LDL by 1.8-fold. In this condition, the contribution of SR-A and SREC-I to the overall degradation of Ac-LDL was 90 and 6%, respectively. LPS increased the absolute contribution of SR-A and SREC-I by 1.9- and 2.3-fold, respectively. On the other hand, LPS decreased the absolute contribution of other pathways by 31%. Consistently, LPS did not increase the expression of other members of the scavenger receptor family such as CD36. In conclusion, SREC-I serves as a major endocytic receptor for Ac-LDL in LPS-stimulated macrophages lacking SR-A, suggesting that it has a key role in the development of atherosclerosis in concert with SR-A.

Scavenger receptors mediate the endocytosis of chemically modified lipoproteins such as acetylated low density lipoprotein (LDL),[1] thereby contributing to the development of atherosclerosis (1). The scavenger receptor gene family comprises a series of unlinked genes encoding membrane proteins with diverse ligand binding activity (2). The class A type I/type II scavenger receptor (SR-A) is the prototype receptor belonging to this family (3) and accounts for ~80% of the uptake of Ac-LDL in macrophages (4, 5).

Recently, we identified scavenger receptor expressed by endothelial cells I (SREC-I), which encodes a protein of 830 amino acids and binds fluorescent DiI-labeled Ac-LDL when expressed in Chinese hamster ovary cells (6), and its paralogous gene, *SREC-II* (7). The SREC-I protein is composed of an N-terminal extracellular ligand binding domain with seven epidermal growth factor receptor-like cysteine pattern signatures, a membrane-spanning domain, and an unusually long C-terminal cytoplasmic domain that includes a Ser/Pro-rich region followed by a Gly-rich region. SREC-II encodes an 834-amino acid protein with 35% homology to SREC-I. Although SREC-II has little activity to internalize modified LDL, SREC-I-expressing fibroblasts are intensely aggregated with SREC-II-expressing fibroblasts, indicating the association of SREC-I and SREC-II (7). However, the precise functions of these two proteins are currently unknown.

In atherosclerotic lesions, macrophages are laden with lipids and immunologically activated (8). In line with this, the development of atherosclerosis is accelerated by LPS (9), a major component of Gram-negative bacteria that stimulates the production of various cytokines *in vivo*, thereby contributing to the pathogenesis of endotoxin shock (10). Conversely, the absence of toll-like receptor 4, a receptor for LPS, inhibits its progression (11). These considerations have prompted us to examine the effects of LPS on the expression of SREC-I. In the present study, we show that LPS robustly stimulated the expression of

* This work was supported by a grant-in-aid for Scientific Research from the Ministry of Education, Science, and Culture and by the Takeda Medical Research Foundation. The costs of publication of this article were defrayed in part by the payment of page charges. This article must therefore be hereby marked "*advertisement*" in accordance with 18 U.S.C. Section 1734 solely to indicate this fact.

¶¶ To whom correspondence should be addressed: Division of Endocrinology and Metabolism, Department of Internal Medicine, Jichi Medical School, 3311-1 Yakushiji, Minamikawachi-machi, Kawachi-gun, Tochigi 329-0498, Japan. Tel.: 81-285-58-7355; Fax: 81-285-40-6035; E-mail: ishibash@jichi.ac.jp.

[1] The abbreviations used are: LDL, low density lipoprotein; SR-A, class A type I/type II scavenger receptor; SR-BI, class B type I scavenger receptor; SREC, scavenger receptor expressed by endothelial cells.

SREC-I in macrophages. In an initial attempt to clarify the role of SREC-I in the uptake of modified lipoproteins as well as in the development of atherosclerosis, we generated mice with targeted disruption of the *SREC-I* gene by homologous recombination in embryonic stem cells. To exclude the overwhelming effect of SR-A on the uptake of Ac-LDL, we further generated mice lacking both SR-A and SREC-I (*SR-A*$^{-/-}$;*SREC-I*$^{-/-}$). By comparing the uptake and degradation of Ac-LDL in peritoneal macrophages isolated from these mice, we found that SREC-I plays a significant role in the uptake of Ac-LDL in the setting of SR-A deficiency, especially when stimulated with LPS. From these results, we propose that SREC-I contributes to the development of atherosclerosis in concert with SR-A.

EXPERIMENTAL PROCEDURES

General Methods—Standard molecular biology techniques were used (12). The current experiments were performed in accordance with institutional guidelines for animal experiments at the University of Tokyo and the Jichi Medical School.

SREC-I Antibody Preparation—Two milligrams of the carboxyl-end peptide of mouse SREC-I (amino acid residues 801–820, KEQEEPLYENVVPMSVPPQH) was conjugated with keyhole limpet hemocyanin using the Imject sulfhydryl-reactive antibody production kit (Pierce). The keyhole limpet hemocyanin-peptide was gel-purified and emulsified with an equal volume of complete Freund's adjuvant (Calbiochem). A female Wister rat was immunized with the emulsions. One week after the boost injection, blood was collected, and the antiserum was purified and eluted through an affinity column (Sulfolink coupling gel; Pierce) to which the antigen peptide was coupled.

Mice—SR-A knock-out mice were generated previously (4). ApoE knock-out mice were purchased from the Jackson Laboratory (Bar Harbor, ME) (13). Both mice had been back-crossed to C57BL/6J genetic background and fed a normal chow diet (MF diet from Oriental Yeast Co., Tokyo, Japan) that contained 5.6% (w/w) fat with 0.09% (w/w) cholesterol, and the mice were allowed access to water and food *ad libitum*.

Cells—Thioglycolate-elicited peritoneal macrophages (14) and mouse embryonic fibroblasts (15) were prepared as described previously. Cells were treated with varying concentrations of LPS (*Escherichia coli* O127:B8; Sigma) for 12 h before the experiments.

Northern Blot Analysis—For the SREC-I cDNA probe, two probes were prepared, namely Probe A, a 5′ 2.0-kb fragment spanning the extracellular and intracellular domains, and Probe B, a 0.1-kb fragment consisting of only the transmembrane domain. Poly (A)$^+$ RNA was purified using Oligotex-dT30^{TM}, an oligo(dT) latex (Roche Applied Science) from 100–150 μg of total RNA that was extracted by TRIzol reagent (Invitrogen) from either cultured cells or tissues. One to three milligrams of poly(A)$^+$ RNA was subjected to 1% agarose gel electrophoresis in the presence of formalin, transferred to Hybond N (Amersham Biosciences), and hybridized to the ^{32}P-labeled probes for SREC-I and other scavenger receptors as described previously (16).

Western Blot Analysis—Cells were lysed with 0.1% SDS. After centrifugation, 50 μg of the supernatant was subjected to SDS-PAGE and transferred to Hybond ECL^{TM}, a nitrocellulose membrane (Amersham Biosciences). After incubation with the anti-SREC-I antibody (1:400 dilution), the membrane was incubated with a goat anti-rat IgG conjugated with horseradish peroxidase (1:2000 dilution; Amersham Biosciences). The secondary antibody was visualized by an enhanced chemiluminescence kit (Amersham Biosciences).

Generation of the SREC-I Knock-out Mice—The *SREC-I* gene was cloned from the 129/Sv mouse genomic library (Clontech) using the mouse cDNA as a probe. A replacement-type targeting vector was constructed so that a 35-bp segment in exon 8, which encodes 3′ two-thirds of the transmembrane domain, was replaced with a polIIneo cassette (Fig. 5*A*). Long arm consists of a 10-kb NotI/KpnI fragment spanning the 5′ untranslated region and exon 8; short arm consists of a 0.9-kb SacI/XbaI fragment within intron 9. These were inserted together into the vector pPolIIshort-neobpA-HSVTK, as described previously (17). After digestion with SalI, the vector was electroporated into JH-1 embryonic stem cells (a generous gift from Dr. Herz at University of Texas Southwestern Medical Center at Dallas, TX). Targeted clones, which had been selected in the presence of G418 and 1-(2-deoxy, 2-fluoro-β-D-arabinofuranosyl)-5 iodouracil, were identified by PCR using the primers 5′-GATTGGGAAGACAATAGCAGGCATGC-3′ and 5′-CAGAGAGTGTCACCACAACAAGAGGA-3′ (Fig. 5*A*). Homologous recombination was verified by Southern blot analysis after digestion with EcoRI using a 0.5-kb SpeI/SmaI fragment, which was downstream of the short arm, as a probe (Fig. 5*A*). Targeted embryonic stem clones were injected into C57BL/6J blastocysts, yielding one line of chimeric mice that transmitted the disrupted allele through the germline.

Generation of the SR-A/SREC-I Double Knock-out Mice—The *SR-A*$^{-/-}$ mice were crossed with the *SREC-I*$^{-/-}$ mice, which were a C57BL/6J × 129/Sv hybrid, to obtain *SR-A*$^{+/-}$;*SREC-I*$^{+/-}$ mice, which were interbred to obtain four types of mice, namely wild-type, *SR-A*$^{+/+}$;*SREC-I*$^{-/-}$, *SR-A*$^{-/-}$;*SREC-I*$^{+/+}$, and *SR-A*$^{-/-}$;*SREC-I*$^{-/-}$ mice. Thus, the genetic background of these mice was 75% C57BL/6J and 25% 129/Sv. Littermates were used for the experiments.

Biochemical Analyses—Blood was collected from the retro-orbital venous plexus after a 12-h fast. Plasma glucose (ANTSENSE II, Bayer Medical, Tokyo, Japan), cholesterol (Determiner TC, Kyowa Medex, Tokyo), and triglycerides (TGLH; Wako Chemicals, Tokyo, Japan) were measured.

Histology—Mice were sacrificed by decapitation. Tissues were excised, fixed in 10% neutral buffered formalin, embedded in paraffin, and stained with hematoxylin-eosin.

Preparation of Lipoproteins—LDL (*d* 1.019–1.063 g/ml) and lipoprotein-deficient serum (*d* >1.21 g/ml) were prepared by stepwise ultracentrifugation from plasma obtained from healthy volunteers. The lipoproteins and lipoprotein-deficient serum were dialyzed against 10 mM sodium phosphate, pH 7.4, 150 mM NaCl, 0.01%(w/v) EDTA, and 0.01% (w/v) NaN_3. LDL was acetylated with acetic anhydrate and radioiodinated by the iodine monochloride method as described (18). Protein concentrations were determined by the BCA protein assay reagent kit (Pierce).

Cellular Uptake and Degradation of ^{125}I-Ac-LDL—Peritoneal macrophages were plated in 12-well plates at a density of 1 × 10^6/well and treated with or without 100 ng/ml of LPS for 12 h. After stringent washing with PBS, the cells were incubated with a medium containing varying concentrations of ^{125}I-Ac-LDL and 5 mg/ml lipoprotein-deficient serum, with or without a 50-fold excess of unlabeled Ac-LDL, for 5 h at 37 °C. The amounts of ^{125}I-Ac-LDL either degraded by or associated with the cells were measured according to a modified method (19) of Goldstein *et al.* (18).

Statistics—The differences of the means were compared by Student's *t* test.

RESULTS

Tissue Distribution of mRNA Expression of SREC-I and -II—We performed Northern blot analyses to examine the expression of SREC-I and II in various organs of a mouse (Fig. 1). SREC-I was expressed in a wide variety of organs, most predominantly in liver, lung, kidney, and heart. On the other hand, the expression of SREC-II was restricted to lung and kidney.

LPS Stimulates the Expression of SREC-I in Peritoneal Macrophages—LPS robustly increased the mRNA expression of both SREC-I and SR-A in macrophages (Fig. 2). The peak of the stimulation was reached by the 12-h time point of the stimulation (Fig. 2*A*), and the maximal responses were obtained at the concentration of 10 ng/ml (Fig. 2*B*). The relative increase in the expression of SREC-I was 4-fold, which was more prominent than that of SR-A (1.8-fold) (Fig. 3). It is of note that the treatment with LPS did not significantly change the expression of MARCO (macrophage receptor with collagenous structure) (20) and SR-BI (21) and that it even decreased the expression of CD36 (22) and FEEL-1 (fasciclin, EGF-like, laminin-type EGF-like, and link domain-containing scavenger receptor-1) (23).

Expression of SREC-I in Aortas—We compared the mRNA expression levels of SREC-I in the atherosclerotic aortas, which were taken from 12-month-old apoE knock-out mice, with normal aortas, mouse embryonic fibroblasts, peritoneal macrophages, kidney, or lung from wild-type mice (Fig. 4). Normal and atherosclerotic aortas expressed 1.7- and 2.1-fold higher levels of SREC-I mRNA than the non-stimulated macrophages, respectively. The expression levels were comparable with those in the kidney, but much lower than those of the LPS-treated macrophages.

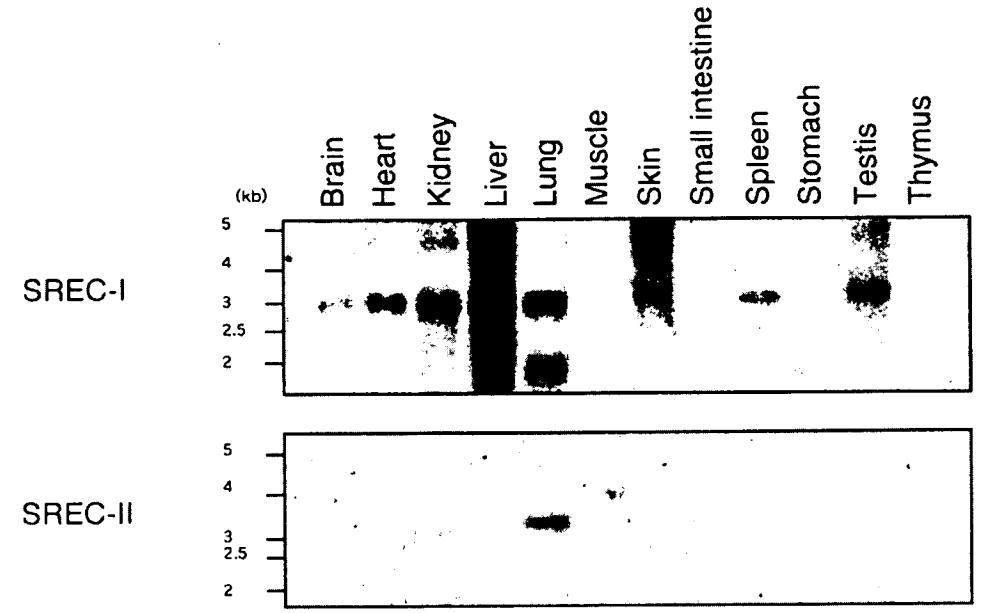

FIG. 1. **Northern blot analysis of SREC-I (*upper panel*) and SREC-II (*lower panel*) in various organs of a mouse.** Two micrograms of poly(A)$^+$ RNA was subjected to Northern blot analysis.

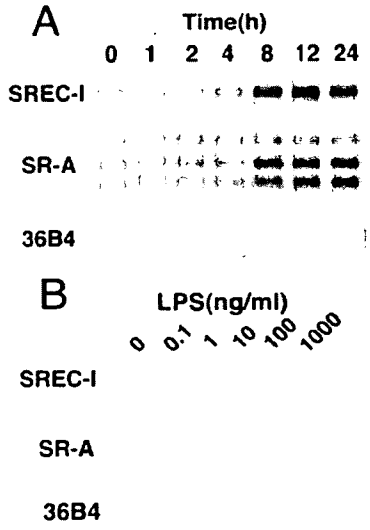

FIG. 2. **Northern blot analysis of SREC-I and SR-A in macrophages treated with LPS.** *A*, thioglycolate-elicited macrophages from C57BL/6 wild-type mice were treated with 100 ng/ml LPS for the indicated times. *B*, cells were treated with the indicated concentrations of LPS for 12 h. Two micrograms of poly(A)$^+$ RNA was subjected to Northern blot analysis. 36B4 was used as a loading control.

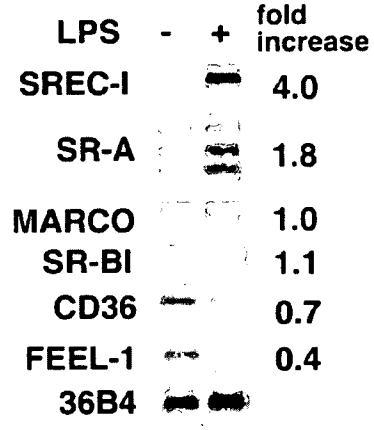

FIG. 3. **Northern blot analysis of scavenger receptors for Ac-LDL in macrophages treated with or without LPS.** Thioglycolate-elicited macrophages from C57BL/6 wild-type mice were treated with (+) or without (−) 100 ng/ml LPS for 12 h. Two micrograms of poly(A)$^+$ RNA was subjected to Northern blot analysis. Probes used were SREC-I, SR-A, MARCO, CD36, SR-BI, and FEEL-1. Signal intensity was corrected against the intensity of 36B4, and the relative signal increase ratio was calculated.

Generation of Mice Lacking the SREC-I and/or SR-A Gene—The intercross of the progeny (*SREC-I*$^{+/-}$) resulted in offspring of both sexes with all three genotypes at the SREC locus with the expected Mendelian ratios (105:191:85 $\chi^2 = 1.06$, $p > 0.05$) (Fig. 5*B*). Fig. 5*C* shows the results of Northern blot analyses of SREC-I in peritoneal macrophages. When hybridized with Probe A, which contains nearly the whole coding region of the SREC-I cDNA, Northern blot revealed a band with mRNA size of 2.9 kb in wild-type macrophages and a band of 2.4 kb in *SREC-I*$^{-/-}$ macrophages. When hybridized with Probe B, which contains the transmembrane domain, no band was detectable in *SREC-I*$^{-/-}$ macrophages. These results indicate that *SREC-I*$^{-/-}$ mice express a truncated transcript that lacks the transmembrane domain. *SREC-I*$^{-/-}$ mice were fertile and apparently normal. There were no significant differences in the growth curves of wild-type and *SREC-I*$^{-/-}$ mice. As shown in Table I, plasma levels of glucose, cholesterol, and triglycerides were not different between wild-type and *SREC-I*$^{-/-}$ mice. We failed to detect any pathological findings in the brain, lung, heart, liver, kidney, and testis of *SREC-I*$^{-/-}$ mice.

Northern blot analysis of four types of mice confirmed the absence of the expression of SR-A in both *SR-A*$^{-/-}$;*SREC-I*$^{+/+}$ and *SR-A*$^{-/-}$;*SREC-I*$^{-/-}$ mice as well as the expression of the disrupted allele of SREC-I in both *SR-A*$^{+/+}$;*SREC-I*$^{-/-}$ and *SR-A*$^{-/-}$;*SREC-I*$^{-/-}$ mice (Fig. 6*A*). Western blot analysis confirmed the absence of SREC-I protein (~140 and160 kDa) in both *SR-A*$^{+/+}$; *SREC-I*$^{-/-}$ and *SR-A*$^{-/-}$;*SREC-I*$^{-/-}$ mice (Fig. 6*B*).

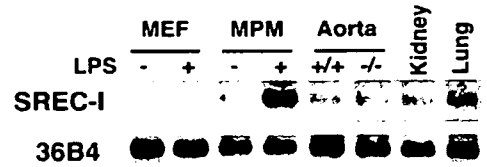

FIG. 4. **Northern blot analysis of SREC-I in normal and atherosclerotic aortas.** RNA were extracted from the following cells or organs: mouse embryonic fibroblasts (*MEF*) treated with (+) or without (−) 100 ng/ml LPS for 12 h; mouse peritoneal macrophages (*MPM*) treated with or without 100 ng/ml LPS for 12 h; kidney; lung; normal aortas from wild-type mice (*Aorta* +/+); and atherosclerotic aortas from apoE−/− mice (*Aorta* −/−). Aortic arches and the thoracic part of descending aortas with rampant visible plaques were excised from five 12-month-old mice. After adipose tissues surrounding the aortas were removed as much as possible, the aortas were used for the preparation of RNA. Three micrograms of poly(A)$^+$ RNA was subjected to Northern blot analysis of SREC-I. 36B4 was used as a loading control.

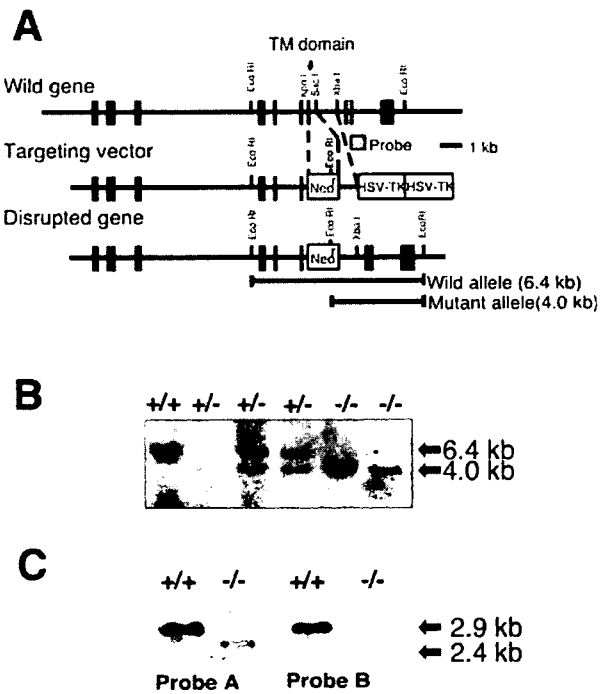

FIG. 5. **Targeted disruption of SREC-I gene.** *A*, map of the SREC-I gene and targeting construct. *Long boxes* represent exons. The exon coding transmembrane domain was replaced with the neomycin resistance gene (*Neo^r*) of targeting vector, which has a herpes simplex virus thymidine kinase (*HSV-TK*) cassette for a negative selection downstream of its short arm. A 0.5-kb fragment was used as a probe for Southern blot analysis (*shaded box*). *B*, Southern blot analysis. After digestion with EcoRI, tail DNA was used for Southern blot analysis. The size of the disrupted allele, 4 kb, was smaller than that of wild-type allele (6.4 kb). *C*, mRNA expression of SREC-I in peritoneal macrophage. Two micrograms of poly(A)$^+$ RNA from wild-type (+/+) and *SREC-I*$^{-/-}$ mice (−/−) macrophage was hybridized with two cDNA probes, namely Probe A, a 5' 2-kb fragment spanning the extracellular and intracellular domains, and Probe B, a 0.1-kb fragment consisting of only the transmembrane domain.

LPS Stimulates Protein Expression of SREC-I—LPS significantly increased the SREC-I protein by ~2-fold in wild-type and *SR-A*$^{-/-}$;*SREC-I*$^{+/+}$ macrophages (Fig. 6*B*).

LPS Increases the Contribution of SREC-I to the Cellular Uptake and Degradation of the ^{125}I-Ac-LDL—In non-stimulated conditions (Fig. 7*A*) there was no significant difference in the specific uptake and degradation of ^{125}I-Ac-LDL between wild-type and *SR-A*$^{+/+}$;*SREC-I*$^{-/-}$ macrophages. Based on the values for 20 μg/ml degraded ^{125}I-Ac-LDL, *SR-A*$^{-/-}$;*SREC-I*$^{+/+}$ macrophages degraded significantly smaller amounts of ^{125}I-Ac-LDL (15%) than did wild-type macrophages, supporting the dominant role of SR-A in the uptake and degradation of ^{125}I-Ac-LDL in macrophages. Compared with *SR-A*$^{-/-}$;*SREC-I*$^{+/+}$ macrophages, *SR-A*$^{-/-}$;*SREC-I*$^{-/-}$ macrophages showed a further reduction in the specific uptake (21%) and degradation of ^{125}I-Ac-LDL (31%). Based on the values for 20 μg/ml degraded ^{125}I-Ac-LDL, the contribution of SR-A and SREC-I to the overall degradation of Ac-LDL was calculated to be 85 and 5%, respectively, in the non-stimulated condition.

LPS increased the uptake and degradation of Ac-LDL by 1.8-fold (Fig. 7*B*). In this condition, there was no significant difference in the specific uptake and degradation of ^{125}I-Ac-LDL between wild-type and *SR-A*$^{+/+}$;*SREC-I*$^{-/-}$ macrophages. Based on the values for 20 μg/ml degraded ^{125}I-Ac-LDL,

TABLE I
Plasma levels of glucose, total cholesterol, and triglycerides

After a 12-h fast, blood was collected from the retro-orbital venous plexus of mice aged 8 weeks. Plasma glucose, total cholesterol, and triglycerides were measured. All values are expressed as means ± S.E. No significant deference between wild-type and *SREC-I*$^{-/-}$ mice.

	Wild-type (+/+)	*SREC-I*$^{-/-}$
	mg/dl	
Glucose	61.1 ± 3.2 (n = 31)	63.2 ± 3.2 (n = 31)
Total cholesterol	89.7 ± 5.1 (n = 22)	82.0 ± 3.3 (n = 27)
Triglycerides	89.6 ± 9.4 (n = 22)	97.4 ± 10.3 (n = 27)

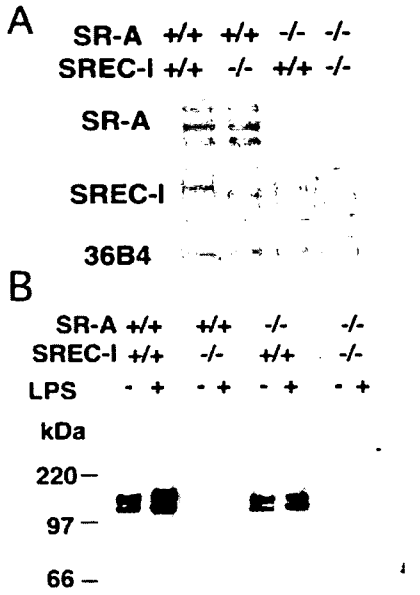

FIG. 6. **Expression of SR-A and SREC-I in macrophages isolated from wild-type, *SR-A*$^{+/+}$;*SREC-I*$^{-/-}$, *SR-A*$^{-/-}$;*SREC-I*$^{+/+}$, and *SR-A*$^{-/-}$;*SREC-I*$^{-/-}$ mice.** Thioglycolate-elicited peritoneal macrophages were prepared from wild-type, *SR-A*$^{+/+}$;*SREC-I*$^{-/-}$, *SR-A*$^{-/-}$;*SREC-I*$^{+/+}$, and *SR-A*$^{-/-}$;*SREC-I*$^{-/-}$ mice. *A*, Northern blot analysis of SR-A and SREC-I. One microgram of poly(A)$^+$ RNA from macrophages was hybridized with SR-A and SREC-I probes (Probe A). *B*, Western blot analysis of SREC-I in macrophages treated with or without LPS. After stimulation with (+) or without (−) 100 ng/ml LPS for 12 h, the cells were lysed with 0.1% SDS, and 50 μg of protein was subjected to SDS-PAGE. Immunoblotting was performed using the rat anti-mouse SREC-I antibody and an enhanced chemiluminescence kit.

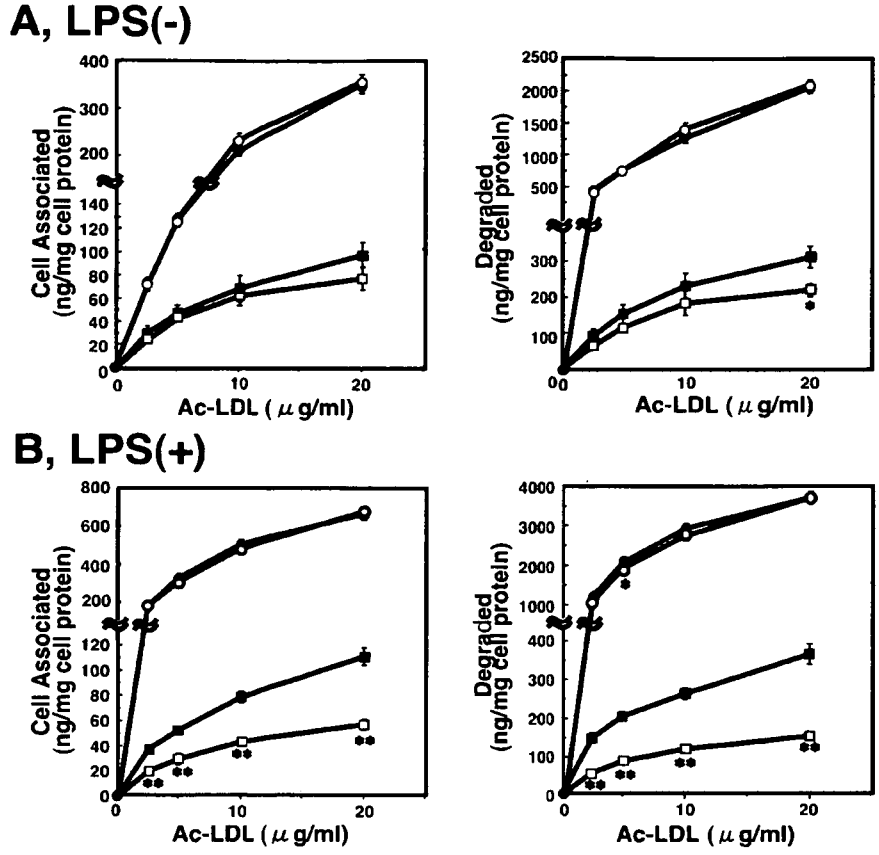

FIG. 7. **Cell association and degradation of ^{125}I-Ac-LDL by peritoneal macrophages isolated from wild-type, *SR-A$^{+/+}$;SREC-I$^{-/-}$*, *SR-A$^{-/-}$;SREC-I$^{+/+}$*, and *SR-A$^{-/-}$;SREC-I$^{-/-}$* mice.** Thioglycolate-elicited peritoneal macrophages were prepared from four types of mice (n = 5), namely wild-type (*solid circle*), *SR-A$^{+/+}$;SREC-I^{-}* (*open circle*), *SR-A$^{-/-}$;SREC-I$^{+/+}$* (*solid square*), and *SR-A$^{-/-}$;SREC-I$^{-/-}$* (*open square*). After treatment with (*panel B*) or without (*panel A*) 100 ng/ml LPS for 12 h, the cells were incubated with the indicated concentrations of ^{125}I-Ac-LDL with or without a 50-fold excess of unlabeled Ac-LDL at 37 °C. After 5 h, the amounts of ^{125}I-Ac-LDL associated or degraded were determined. Specific values were calculated by subtracting the nonspecific values from the total values. All values are expressed as means ± S.E. of five mice. *, $p < 0.05$ *versus SR-A$^{-/-}$;SREC-I$^{+/+}$* mice; **, $p < 0.01$ *versus SR-A$^{-/-}$; SREC-I$^{+/+}$* mice.

SR-A$^{-/-}$;SREC-I$^{+/+}$ macrophages degraded significantly smaller amounts of ^{125}I-Ac-LDL (10%) than did wild-type macrophages. Compared with *SR-A$^{-/-}$;SREC-I$^{+/+}$* macrophages, *SR-A$^{-/-}$;SREC-I$^{-/-}$* macrophages showed a further reduction in the specific uptake (49%) and degradation of ^{125}I-Ac-LDL (59%). Based on the values for 20 μg/ml degraded Ac-LDL, the contribution of SR-A and SREC-I to the overall degradation of ^{125}I-Ac-LDL was calculated to be 90 and 6%, respectively. LPS increased the absolute contribution of SR-A and SREC-I by 1.9- and 2.3-fold, respectively. On the other hand, LPS decreased the absolute contribution of other pathways by 31%.

DISCUSSION

In the present study, we have first shown that SREC-I, a novel member of the scavenger receptor family that recognizes modified lipoproteins, is expressed in a wide variety of tissues including macrophages and aortas, implicating its involvement in the development of atherosclerosis. The expression of SREC-I was not significantly different between normal and atherosclerotic aortas, although it was robustly induced by LPS in macrophages, a major cell type that is present in foam cell lesions. To define the precise role of SREC-I, we have generated wild-type, *SR-A$^{+/+}$;SREC-I$^{-/-}$*, *SR-A$^{-/-}$;SREC-I$^{+/+}$*, and *SR-A$^{-/-}$;SREC-I$^{-/-}$* mice and compared the uptake and degradation of Ac-LDL in macrophages between these mice. Results show that the contribution of SREC-I to the overall uptake and degradation of Ac-LDL was 5% in the non-stimulated condition and 6% in the LPS-stimulated condition. Although the involvement of SREC-I was relatively small compared with that of SR-A, LPS increased the SREC-I mediated degradation by 2.3-fold, which accounted for 60% of the amounts of Ac-LDL degraded by the pathway independent of SR-A.

Because the responses of scavenger receptors to LPS are variable, we did not expect that LPS induced the expression of SREC-I in macrophages. LPS induces SR-A expression in mouse macrophages, which was confirmed in our experiments (Figs. 2 and 3) but not in THP-1 monocyte/macrophages (24) and human monocyte-derived macrophages (25). Because SR-A is able to bind LPS (26), the induction of SR-A by LPS may have a protective role against endotoxemia. This notion is in line with the susceptibility of SR-A knock-out mice to endotoxin shock (4, 27, 28). On the other hand, LPS down-regulates SR-B1 expression (29), which was confirmed in our experiments (Fig. 2).

The mechanism by which LPS induces SREC-I is intriguing. It is well known that LPS modulates gene expression though the activation of NF-κB signaling (30), and some of the effects are mediated by proinflammatory cytokines, whose expression is stimulated by LPS. However, there is no NF-κB binding site in the 5′-flanking region of the human SREC-I gene 1 kb upstream of the transcription initiation site (31). Furthermore,

LPS did not induce SREC-I expression in human umbilical vein endothelial cells, and tumor necrosis factor-α did not have increasing effects on SREC-I expression in mouse macrophages (data not shown). Further studies are warranted to decipher how LPS induces SREC-I expression.

Although SREC-I is expressed in macrophages, particularly when stimulated with LPS, there was no significant difference in the expression levels between normal and atherosclerotic aortas (Fig. 4). This suggests that other cell types such as endothelial cells and smooth muscle cells in the aortas express comparable levels of SREC-I.

SR-A is the major pathway for the uptake and degradation of Ac-LDL, accounting for 80% of the total activity (4, 5). Because other scavengers are expressed in macrophages (Fig. 2) and are able to bind Ac-LDL (2), the question is which scavenger receptor is the second most important in the uptake and degradation of Ac-LDL. Our results have revealed that the role of SREC-I is relatively minor in the non-stimulated macrophages, which is largely consistent with the recent report by Kunjathoor *et al.* (22). According to them, SR-A and CD36 account for 75–90% of the total amounts of chemically modified LDL degraded by macrophages. In SR-A-deficient macrophages stimulated with LPS, however, the absolute contribution of SREC-I was significantly increased by 2.3-fold, accounting for 60% of the SR-A-independent uptake and degradation of Ac-LDL (Fig. 7*B*). The degree of increase in the SREC-I mediated uptake and degradation of Ac-LDL is largely comparable with that in SREC-I protein expression (Fig. 6*B*). It is interesting to note that LPS decreased the absolute contribution of the other endocytic pathway, which is independent of either SR-A or SREC-I, by 31%. This finding is consistent with the Northern blot results that show that LPS did not significantly increase the expression of the other members of scavenger receptor family such as MARCO, SR-BI, CD36, and FEEL-1 (Fig. 3). Thus, SREC-I is the second most important receptor mediating the uptake of Ac-LDL, at least in macrophages stimulated with LPS. Given the activated state of macrophages in rupture-prone unstable plaques (8), particularly in plaques infected with microorganisms such as *Chlamydia*, which is associated with an increased prevalence of coronary events (32), SREC-I may take a significant part in the foam cell formation in these pathological conditions. Other aspects of LPS may be involved in the atherogenesis. For example, Baranova *et al.* (29) and Khovidhunkit *et al.* (33) have recently reported that LPS inhibits high density lipoprotein-mediated cholesterol efflux via down-regulation of the expression of ABCA1 and ABCG1. These observations are consistent not only with the ability of LPS to stimulate lipid accumulation in macrophages *in vitro* (34) but also with the proatherogenic effects of LPS (9) and its cognate receptor, Toll-like receptor 4, *in vivo* (11).

Functions of adhesion molecules have been assigned to both SR-A and SREC-I/II. Chinese hamster ovary cells overexpressing SR-A have an increased ability to adhere to plastic surfaces (35). Likewise, intense aggregation was observed when SREC-I-expressing fibroblast L-cells were mixed with those expressing SREC-II (7). Thus, it is reasonable to speculate that *SREC-I*$^{-/-}$ mice have some phenotypes with regard to cell adhesion. However, there were no obvious abnormalities in the pathologies (data not shown).

The precise roles of scavenger receptors in atherogenesis have been tested only for SR-A and CD36. With regard to SR-A, we (4, 36, 37) and Babaev *et al.* (38) have reported that SR-A deficiency protects against the development of atherosclerosis in either apoE, LDL receptor-deficient, or wild-type mice. de Winther *et al.* (39), however, recently reported apparently opposite results, *i.e.* SR-A deficiency leads to more complex lesions in the APOE3Leiden mice. The same group reported the reduction in atherosclerosis in LDL receptor knock-out mice in which SR-A was overexpressed in a macrophage-specific manner (40). These contradictory results could be attributed to the broad repertoire of functions and the widespread expression of SR-A (41). With regard to CD36, Febbraio *et al.* have reported that CD36 deficiency protects against atherosclerosis in an apoE-deficient background (42). Availability of the *SR-A*$^{-/-}$; *SREC-I*$^{-/-}$ mice should allow us to determine the role of SREC-I in the development of atherosclerosis by crossing with the genetically hyperlipidemic mice, for example. If the hypothesis is correct, SREC-I should be a new target for preventing atherosclerosis.

Acknowledgments—We thank Kimiko Saito, Megumi Herai, Mihoko Kusubae, and Rie Tamura for excellent technical assistance. We also thank Tetsuya Kitamine, Stephane Perrey, Michiyo Amemiya-Kudo, and Takanari Gotoda for helpful comments and discussion.

REFERENCES

1. Brown, M. S., and Goldstein, J. L. (1983) *Annu. Rev. Biochem.* **52,** 223–261
2. Krieger, M. (1997) *Curr. Opin. Lipidol.* **8,** 275–280
3. Kodama, T., Freeman, M., Rohrer, L., Zabrecky, J., Matsudaira, P., and Krieger, M. (1990) *Nature* **343,** 531–535
4. Suzuki, H., Kurihara, Y., Takeya, M., Kamada, N., Kataoka, M., Jishage, K., Ueda, O., Sakaguchi, H., Higashi, T., Suzuki, T., Takashima, Y., Kawabe, Y., Cynshi, O., Wada, Y., Honda, M., Kurihara, H., Aburatani, H., Doi, T., Matsumoto, A., Azuma, S., Noda, T., Toyoda, Y., Itakura, H., Yazaki, Y., Horiuchi, S., Takahashi, K., Kruijt, J. K., Van Berkel, T. J. C., Steinbrecher, U. P., Ishibashi, S., Maeda, N., Gordon, S., and Kodama, T. (1997) *Nature* **386,** 292–296
5. Lougheed, M., Lum, C. M., Ling, W., Suzuki, H., Kodama, T., and Steinbrecher, U. (1997) *J. Biol. Chem.* **272,** 12938–12944
6. Adachi, H., Tsujimoto, M., Arai, H., and Inoue, K. (1997) *J. Biol. Chem.* **272,** 31217–31220
7. Ishii, J., Adachi, H., Aoki, J., Koizumi, H., Tomita, S., Suzuki, T., Tsujimoto, M., Inoue, K., and Arai, H. (2002) *J. Biol. Chem.* **277,** 39696–39702
8. Libby, P. (2002) *Nature* **420,** 868–874
9. Lehr, H. A., Sagban, T. A., Ihling, C., Zahringer, U., Hungerer, K. D., Blumrich, M., Reifenberg, K., and Bhakdi, S. (2001) *Circulation* **104,** 914–920
10. Lynn, W. A., and Cohen, J. (1995) *Clin. Infect. Dis.* **20,** 143–158
11. Vink, A., Schoneveld, A. H., van der Meer, J. J., van Middelaar, B. J., Sluijter, J. P., Smeets, M. B., Quax, P. H., Lim, S. K., Borst, C., Pasterkamp, G., and de Kleijn, D. P. (2002) *Circulation* **106,** 1985–1990
12. Sambrook, J., and Russell, D. W. (2001) *Molecular Cloning: A Laboratory Manual*, Cold Spring Harbor Laboratory Press, Cold Spring Harbor, NY
13. Zhang, S. H., Reddick, R. L., Piedrahita, J. A., and Maeda, N. (1992) *Science* **258,** 468–471
14. Yagyu, H., Kitamine, T., Osuga, J., Tozawa, R., Chen, Z., Kaji, Y., Oka, T., Perrey, S., Tamura, Y., Ohashi, K., Okazaki, H., Yahagi, N., Shionoiri, F., Iizuka, Y., Harada, K., Shimano, H., Yamashita, H., Gotoda, T., Yamada, N., and Ishibashi, S. (2000) *J. Biol. Chem.* **275,** 21324–21330
15. Okazaki, H., Osuga, J., Tamura, Y., Yahagi, N., Tomita, S., Shionoiri, F., Iizuka, Y., Ohashi, K., Harada, K., Kimura, S., Gotoda, T., Shimano, H., Yamada, N., and Ishibashi, S. (2002) *Diabetes* **51,** 3368–3375
16. Tamura, Y., Adachi, H., Osuga, J., Ohashi, K., Yahagi, N., Sekiya, M., Okazaki, H., Tomita, S., Iizuka, Y., Shimano, H., Nagai, R., Kimura, S., Tsujimoto, M., and Ishibashi, S. (2003) *J. Biol. Chem.* **278,** 12613–12617
17. Ishibashi, S., Brown, M. S., Goldstein, J. L., Gerard, R. D., Hammer, R. E., and Herz, J. (1993) *J. Clin. Investig.* **92,** 883–893
18. Goldstein, J. L., Basu, S. K., and Brown, M. S. (1983) *Methods Enzymol.* **98,** 241–260
19. Perrey, S., Ishibashi, S., Kitamine, T., Osuga, J., Yagyu, H., Chen, Z., Shionoiri, F., Iizuka, Y., Yahagi, N., Tamura, Y., Ohashi, K., Harada, K., Gotoda, T., and Yamada, N. (2001) *Atherosclerosis* **154,** 51–60
20. Elomaa, O., Kangas, M., Sahlberg, C., Tuukkanen, J., Sormunen, R., Liakka, A., Thesleff, I., Kraal, G., and Tryggvason, K. (1995) *Cell* **80,** 603–609
21. Acton, S. L., Scherer, P. E., Lodish, H. F., and Krieger, M. (1994) *J. Biol. Chem.* **269,** 21003–21009
22. Kunjathoor, V. V., Febbraio, M., Podrez, E. A., Moore, K. J., Andersson, L., Koehn, S., Rhee, J. S., Silverstein, R., Hoff, H. F., and Freeman, M. W. (2002) *J. Biol. Chem.* **277,** 49982–49988
23. Adachi, H., and Tsujimoto, M. (2002) *J. Biol. Chem.* **277,** 34264–34270
24. Fitzgerald, M. L., Moore, K. J., Freeman, M. W., and Reed, G. L. (2000) *J. Immunol.* **164,** 2692–2700
25. van Lenten, B. J., and Fogelman, A. M. (1992) *J. Immunol.* **148,** 112–116
26. Hampton, R. Y., Golenbock, D. T., Penman, M., Krieger, M., and Raetz, C. R. (1991) *Nature* **352,** 342–344
27. Haworth, R., Platt, N., Keshav, S., Hughes, D., Darley, E., Suzuki, H., Kurihara, Y., Kodama, T., and Gordon, S. (1997) *J. Exp. Med.* **186,** 1431–1439
28. Ishiguro, T., Naito, M., Yamamoto, T., Hasegawa, G., Gejyo, F., Mitsuyama, M., Suzuki, H., and Kodama, T. (2001) *Am. J. Pathol.* **158,** 179–188
29. Baranova, I., Vishnyakova, T., Bocharov, A., Chen, Z., Remaley, A. T., Stonik, J., Eggerman, T. L., and Patterson, A. P. (2002) *Infect Immun.* **70,** 2995–3003
30. Muller, J. M., Ziegler-Heitbrock, H. W., and Baeuerle, P. A. (1993) *Immunobiology* **187,** 233–256

31. Adachi, H., and Tsujimoto, M. (2002) *J. Biol. Chem.* **277,** 24014–24021
32. Becker, A. E., de Boer, O. J., and van Der Wal, A. C. (2001) *Annu. Rev. Med.* **52,** 289–297
33. Khovidhunkit, W., Moser, A. H., Shigenaga, J. K., Grunfeld, C., and Feingold, K. R. (2001) *J. Lipid Res.* **42,** 1636–1644
34. Funk, J. L., Feingold, K. R., Moser, A. H., and Grunfeld, C. (1993) *Atherosclerosis* **98,** 67–82
35. Fraser, I., Hughes, D., and Gordon, S. (1993) *Nature* **364,** 343–346
36. Sakaguchi, H., Takeya, M., Suzuki, H., Hakamata, H., Kodama, T., Horiuchi, S., Gordon, S., van der Laan, L. J., Kraal, G., Ishibashi, S., Kitamura, N., and Takahashi, K. (1998) *Lab. Investig.* **78,** 423–434
37. Kamada, N., Kodama, T., and Suzuki, H. (2001) *J. Atheroscler. Thromb.* **8,** 1–6
38. Babaev, V. R., Gleaves, L. A., Carter, K. J., Suzuki, H., Kodama, T., Fazio, S., and Linton, M. F. (2000) *Arterioscler. Thromb. Vasc. Biol.* **20,** 2593–2599
39. de Winther, M. P., Gijbels, M. J., van Dijk, K. W., van Gorp, P. J., Suzuki, H., Kodama, T., Frants, R. R., Havekes, L. M., and Hofker, M. H. (1999) *Atherosclerosis* **144,** 315–321
40. de Winther, M. P., Gijbels, M. J., van Dijk, K. W., Havekes, L. M., and Hofker, M. H. (2000) *Int. J. Tissue React.* **22,** 85–91
41. Platt, N., and Gordon, S. (2001) *J. Clin. Investig.* **108,** 649–654
42. Febbraio, M., Podrez, E. A., Smith, J. D., Hajjar, D. P., Hazen, S. L., Hoff, H. F., Sharma, K., and Silverstein, R. L. (2000) *J. Clin. Investig.* **105,** 1049–1056